Electron and Hydrogen-Atom Self-Exchange Reactions of Iron and Cobalt Coordination Complexes

Jeffrey C. Yoder, Justine P. Roth,*[†] Emily M. Gussenhoven, Anna S. Larsen, and James M. Mayer*

Contribution from the Department of Chemistry, University of Washington, Box 351700, Seattle, Washington 98195-1700

Received June 20, 2002 ; E-mail: jproth@eve.cchem.berkeley.edu; mayer@chem.washington.edu

Abstract: Reported here are self-exchange reactions between iron 2,2′-bi(tetrahydro)pyrimidine (H_2bip) complexes and between cobalt 2,2′-biimidazoline (H_2bim) complexes. The ^1H NMR resonances of $[Fe^{II}(H_2bip)_3]^{2+}$ are broadened upon addition of $[Fe^{III}(H_2bip)_3]^{3+}$, indicating that electron self-exchange occurs with $k_{Fe,e-} = (1.1 \pm 0.2) \times 10^5$ M^{-1} s^{-1} at 298 K in CD_3CN. Similar studies of $[Fe^{II}(H_2bip)_3]^{2+}$ plus $[Fe^{III}(Hbip)(H_2bip)_2]^{2+}$ indicate that hydrogen-atom self-exchange (proton-coupled electron transfer) occurs with $k_{Fe,H•} = (1.1 \pm 0.2) \times 10^4$ M^{-1} s^{-1} under the same conditions. Both self-exchange reactions are *faster* at lower temperatures, showing small negative enthalpies of activation: $\Delta H^{\ddagger}(e^-) = -2.1 \pm 0.5$ kcal mol^{-1} (288–320 K) and $\Delta H^{\ddagger}(H•) = -1.5 \pm 0.5$ kcal mol^{-1} (260–300 K). This behavior is concluded to be due to the faster reaction of the low-spin states of the iron complexes, which are depopulated as the temperature is raised. Below about 290 K, rate constants for electron self-exchange show the more normal decrease with temperature. There is a modest kinetic isotope effect on H-atom self-exchange of 1.6 ± 0.5 at 298 K that is close to that seen previously for the fully high-spin iron biimidazoline complexes.[12] The difference in the measured activation parameters, $E_a^D - E_a^H$, is -1.2 ± 0.8 kcal mol^{-1}, appears to be inconsistent with a semiclassical view of the isotope effect, and suggests extensive tunneling. Reactions of $[Co(H_2bim)_3]^{2+}$-d_{24} with $[Co(H_2bim)_3]^{3+}$ or $[Co(Hbim)(H_2bim)_2]^{2+}$ occur with scrambling of ligands indicating inner-sphere processes. The self-exchange rate constant for outer-sphere electron transfer between $[Co(H_2bim)_3]^{2+}$ and $[Co(H_2bim)_3]^{3+}$ is estimated to be 10^{-6} M^{-1} s^{-1} by application of the Marcus cross relation. Similar application of the cross relation to H-atom transfer reactions indicates that self-exchange between $[Co(H_2bim)_3]^{2+}$ and $[Co(Hbim)(H_2bim)_2]^{2+}$ is also slow, $\leq 10^{-3}$ M^{-1} s^{-1}. The slow self-exchange rates for the cobalt complexes are apparently due to their interconverting high-spin $[Co^{II}(H_2bim)_3]^{2+}$ with low-spin Co(III) derivatives.

Introduction

Self-exchange reactions involve degenerate transfer of a particle or group between two species. Rates of electron self-exchange, k_{XX} for $X + X^+ \rightleftarrows X^+ + X$, have played a prominent role in the development of electron-transfer theory because they are a measure of intrinsic barriers and because they appear in the Marcus cross relation, eq 1.[1] Equation 1 expresses the rate

$$k_{XY} = \sqrt{k_{XX}k_{YY}K_{XY}f_{XY}} \qquad (1)$$

constant of a cross reaction (k_{XY}) as a function of the rate constants for the constituent self-exchange reactions (k_{XX} and k_{YY}), the equilibrium constant (K_{XY}), and a factor f_{XY} which is close to 1 for reactions of moderate driving force.[1,2] Although recent quantum mechanical treatments of electron transfer do

not readily yield the cross relation,[3] it has been shown to hold for a variety of reactions in both adiabatic and nonadiabatic regimes.[1,4]

Marcus–Hush theory and the cross relation were developed for electron-transfer reactions between weakly interacting species, but they have seen increasing application to reactions which involve bond rupture and formation,[5] including hydride[6] and proton transfers.[7] We have recently reported that rate constants for a range of hydrogen-atom transfer reactions (eq 2) follow the cross relation.[8] Organic hydrogen-atom transfer reactions

† Current address: Department of Chemistry, University of California, Berkeley, CA 94720.

(1) (a) Marcus, R. A. *Discuss. Faraday Soc.* **1960**, *29*, 21. (b) Marcus, R. A. *Angew. Chem., Int. Ed. Engl.* **1993**, *32*, 1111. (c) Marcus, R. A.; Sutin, N. *Biochim. Biophys. Acta* **1985**, *811*, 265. (d) Sutin, N. *Prog. Inorg. Chem.* **1983**, *30*, 441–499. (e) Bolton, J. R.; Archer, M. D. In *Electron Transfer in Inorganic, Organic, and Biological Systems*; Bolton, J. R. et al., Eds.; *Adv. Chem. Ser.*; American Chemical Society: Washington, DC, 1991; Vol. 228, p 7. (f) Albery, W. J. *Ann. Rev. Phys. Chem.* **1980**, *31*, 227.

(2) ln $f_{XY} = [\ln K_{XY}]^2[4 \ln(k_{XX}k_{YY}Z^{-2})]^{-1}$ (neglecting work terms); Z is the collisional frequency.[1c,d]
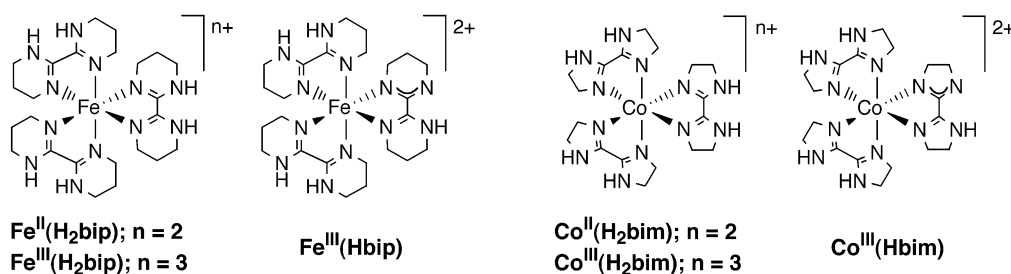
(3) (a) Barbara, P. F.; Meyer, T. J.; Ratner, M. A. *J. Phys. Chem.* **1996**, *100*, 13148. (b) Bixon, M; Jortner, J. *Adv. Chem. Phys.* **1999**, *106*, 35.

(4) Nelsen, S. F.; Trieber, D. A., II; Nagy, M. A.; Konradsson, A.; Halfen, D. T.; Splan, K. A.; Pladziewicz, J. R. *J. Am. Chem. Soc.* **2000**, *122*, 5940.

(5) (a) Marcus, R. A. *J. Phys. Chem.* **1968**, *72*, 891. (b) Cohen, A. O.; Marcus, R. A. *J. Phys. Chem.* **1968**, *72*, 4249. (c) Guthrie, J. P. *J. Am. Chem. Soc.* **1997**, *119*, 1151–1152. (d) Lewis, E. S.; Hu, D. D. *J. Am. Chem. Soc.* **1984**, *106*, 3292. (e) Pellerite, M. J.; Brauman, J. I. *J. Am. Chem. Soc.* **1983**, *105*, 2672. (f) Endicott, J. F.; Balakrishnan, K. P.; Wong, C.-L. *J. Am. Chem. Soc.* **1980**, *102*, 5519. (g) Richard, J. P.; Amyes, T. L.; Williams, K. B. *Pure Appl. Chem.* **1998**, *70*, 2007.

(6) (a) Kreevoy, M. M.; Oh, S. *J. Am. Chem. Soc.* **1973**, *95*, 4805. (b) Kreevoy, M. M.; Ostović, D.; Han Lee, I.-S.; Binder, D. A.; King, G. W. *J. Am. Chem. Soc.* **1988**, *110*, 524. (c) Roberts, R. M. G.; Ostović, D.; Kreevoy, M. M. *Faraday Discuss. Chem. Soc.* **1982**, *74*, 257–265.

Chart 1

$Fe^{II}(H_2bip)$; n = 2
$Fe^{III}(H_2bip)$; n = 3

$Fe^{III}(Hbip)$

$Co^{II}(H_2bim)$; n = 2
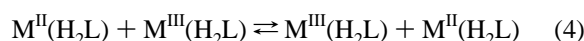$Co^{III}(H_2bim)$; n = 3

$Co^{III}(Hbim)$

have been intensively studied because of their importance in many chemical processes, from combustion and the production of commodity chemicals[9] to various biological transformations.[10] A vast number of H-atom transfer rate constants have been measured, but only for a limited number of self-exchange reactions (eq 3) or for reactions involving transition metal complexes.[11,12] The traditional framework for understanding

$$X + H-Y \xrightarrow{k_{XY}} X-H + Y \qquad (2)$$

$$X + H-X \xrightarrow{k_{XX}} X-H + X \qquad (3)$$
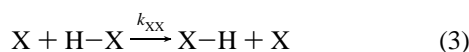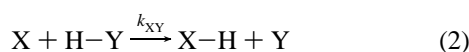
H-atom transfer rates is the Bell–Evans–Polanyi equation, $\Delta H^{\ddagger} = \alpha \Delta H + \beta$,[13] which can be viewed as a corollary to the Marcus equation[14] and has been shown to apply to reactions of transition metal complexes.[15]

Described here are studies of iron 2,2′-bi(tetrahydropyrimidine) (H$_2$bip) and cobalt 2,2′-biimidazoline (H$_2$bim) complexes, extending our previous work on the iron-H$_2$bim system.[12] The compounds are shown in Chart 1, which also gives the abbreviations used. Reactions between the fully protonated divalent and trivalent derivatives (eq 4) are electron self-exchange processes. Exchange between $M^{II}(H_2L)$ and $M^{III}(HL)$ (eq 5) involves transfer of both a proton and an electron, and these reactions can be described either as hydrogen-atom transfer or as proton-coupled electron transfer (PCET). PCET is a subject

$$M^{II}(H_2L) + M^{III}(H_2L) \rightleftharpoons M^{III}(H_2L) + M^{II}(H_2L) \qquad (4)$$

$$M^{II}(H_2L) + M^{III}(HL) \rightleftharpoons M^{III}(HL) + M^{II}(H_2L) \qquad (5)$$

of much current interest,[12,16] and the iron/biimidazoline system has been examined both experimentally[12] and theoretically.[16d] In this report, reactions 5 will be (somewhat arbitrarily) described as hydrogen-atom transfers because we have found a close analogy between these reactions and organic H-atom transfer processes.[8,15,17] The cobalt complexes undergo very slow self-exchange, for both electron and H-atom transfer, consistent with many previous studies of the interconversion of high-spin Co(II) and low-spin Co(III).[18] In the iron/H$_2$bip system, the self-exchange reactions are quite facile and have negative activation energies over a portion of the temperature range studied. In both systems, there is a close relationship between hydrogen-atom/PCET self-exchange and electron self-exchange.

Results

I. Description of Compounds. Syntheses of the three iron compounds have been previously described.[19] The ^{1}H NMR spectrum of **$Fe^{II}(H_2bip)$** at ambient temperatures shows broad resonances [full widths at half maximum (fwhm) 140–360 Hz] for the amine protons (δ 75.1, confirmed by exchange with MeOD) and six separate CH signals (δ −1.5 to 22.5). The observation of six inequivalent methylene protons indicates a D_3-symmetrical structure that is stereochemically rigid on the NMR time scale. Measurements of the magnetic susceptibility in acetonitrile solution using the Evans method[20] indicate that **$Fe^{II}(H_2bip)$** exists as a mixture of high- and low-spin states.[21] The μ_{eff} for the **$Fe^{II}(H_2bip)$** ranges from 3.4 μ_B at 239 K to 5.0 μ_B at 322 K (Figure 1), the latter being close to that expected for a high-spin iron(II).[22] The measured moments were independent of sample preparation, deuteration of the NH positions,

(7) (a) Kristjánsdóttir, S. S.; Norton, J. R. *J. Am. Chem. Soc.* **1991**, *113*, 4366. (b) For leading references, see: Guthrie, J. P. *J. Am. Chem. Soc.* **1996**, *118*, 12886−12890.

(8) Roth, J. P.; Yoder, J. C.; Won, T.-J.; Mayer, J. M. *Science* **2001**, *294*, 2524.

(9) Olah, G. A.; Molnár, Á. *Hydrocarbon Chemistry*; Wiley: New York, 1995.

(10) (a) Stubbe, J.; van der Donk, W. A. *Chem. Rev.* **1998**, *98*, 705. (b) Sono, M.; Roach, M. P.; Coulter, E. D.; Dawson, J. H. *Chem. Rev.* **1996**, *96*, 2841. (c) Que, L., Jr.; Ho, R. Y. N. *Chem. Rev.* **1996**, *96*, 2607. (d) Wallar, B. J.; Lipscomb, J. D. *Chem. Rev.* **1996**, *96*, 2625. (e) Klinman, J. P. *Chem. Rev.* **1996**, *96*, 2541. (f) Tommos, C.; Babcock, G. T. *Biochim. Biophys. Acta-Bioenerg.* **2000**, *199*, 1458. (g) Burton, G. W.; Ingold, K. U. *Acc. Chem. Res.* **1986**, *19*, 194−201.

(11) *Radical Reaction Rates in Liquids*; Landolt-Börnstein New Series; Fischer, H., Ed.; Springer Verlag: New York, 1984; Vol. 13, subvols. a−e, and Vol. 18, subvols. A−E.

(12) Roth, J. P.; Lovell, S.; Mayer, J. M. *J. Am. Chem. Soc.* **2000**, *122*, 5486.

(13) *Free Radicals*; Kochi, J. K., Ed.; Wiley: New York, 1973, especially Ingold, K. U. Chapter 2, Vol. 1, pp 69ff and Russell, G. A. Chapter 7, Vol. 1, pp 283−293.

(14) (a) Shaik, S. S.; Schlegel, H. B.; Wolfe, S. *Theoretical Aspects of Physical Organic Chemistry: The S_N2 Mechanism*; Wiley: New York, 1992; Chapter 1. (b) Farrer, B. T.; Thorp, H. H. *Inorg. Chem.* **1999**, *38*, 2497−2502. (c) References 2c, 5c, and 12.

(15) (a) Mayer, J. M. *Acc. Chem. Res.* **1998**, *31*, 441. (b) Gardner, K. A.; Mayer, J. M. *Science* **1995**, *269*, 1849. (c) For a counterexample, see: Goldsmith, C. R.; Jonas, R. T.; Stack, T. P. D. *J. Am. Chem. Soc.* **2002**, *124*, 83−96.

(16) (a) Hammes-Schiffer, S. *Acc. Chem. Res.* **2001**, *34*, 273. (b) Cukier, R. I.; Nocera, D. G. *Annu. Rev. Phys. Chem.* **1998**, *49*, 337. (c) Cukier, R. I. *J. Phys. Chem. B* **2002**, *106*, 1746−1757. (d) Iordanova, N.; Decornez, H.; Hammes-Schiffer, S. *J. Am. Chem. Soc.* **2001**, *123*, 3723. (e) Kuznetsov, A. M.; Ulstrup, J. *Can. J. Chem.* **1999**, *77*, 1085−1096. (f) Krishtalik, L. I. *Biochim. Biophys. Acta* **2000**, *1458*, 6−27. (g) Kotelnikov, A. I.; Medvedev, E. S.; Medvedev, D. M.; Stuchebrukhov, A. A. *J. Phys. Chem. B* **2001**, *105*, 5789−5796.

(17) Roth, J. P.; Mayer, J. M. *Inorg. Chem.* **1999**, *38*, 2760.

(18) For selected studies and leading references, see refs 1d, pp 490ff, 24, and: (a) Swaddle, T. W. *Can. J. Chem.* **1996**, *74*, 631−8. (b) Sutin, N.; Brunschwig, B. S.; Creutz, C.; Winkler, J. R. *Pure Appl. Chem.* **1988**, *60*, 1817−1830.

(19) Burnett, M. G.; McKee, V.; Nelson, S. M. *J. Chem. Soc., Dalton Trans.* **1981**, 1492.

(20) (a) Sur, S. K. *J. Magn. Reson.* **1989**, *82*, 169−173. (b) Live, D. H.; Chan, S. I. *Anal. Chem.* **1970**, *42*, 791−792. (c) Evans, D. F. *J. Chem. Soc.* **1959**, 2003.

(21) Our data contrast with the original report[19] that **$Fe^{II}(H_2bip)$** is a 1:1 mixture of high-spin and low-spin forms at room temperature, based on the solid-state magnetic moment of 2.6 μ_B and the observation that the intensities of the two optical absorption bands at 510 and 580 nm (in MeCN) had opposite temperature dependencies. We find that various batches of **$Fe^{II}(H_2bip)$** have λ_{max} = 510 nm with a shoulder at 580 nm and that both bands decrease in intensity with increasing temperature between 283 and 343 K (cooling reproduces the original spectrum).

(22) Greenwood, N. N.; Earnshaw, A. *Chemistry of the Elements*, 2nd ed.; Butterworth-Heinemann: Oxford, 1997; pp 1090, 1092.
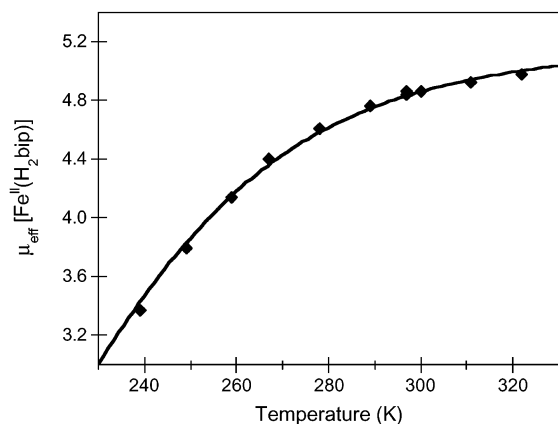
Figure 1. A plot of μ_{eff} versus temperature for **Fe^{II}(H$_2$bip)-d_6** (◆). The line is calculated using $\Delta H° = -5.1$ kcal mol^{-1}, $\Delta S° = -21$ eu, and the limiting μ_{eff}(high-spin) = 5.2 μ_B.

Table 1. High-Spin/Low-Spin Equilibria for Iron 2,2′-Bi(tetrahydro)pyrimidine Complexes^a

	μ_{eff} (298 K)^b	K_{eq} (298 K)^c	μ_{eff} (240–320 K)^b	$\Delta H°$ ^{d}	$\Delta S°$ ^{e}
Fe^{II}(H$_2$bip)^f	4.9	0.15	3.4–5.0	-5.1 ± 0.5	-21 ± 2
Fe^{III}(H$_2$bip)^g	3.2	3.9	2.6–3.5	-2.8 ± 0.3	-7 ± 1
Fe^{III}(Hbip)	3.2	4.6	2.8–3.4	-1.9 ± 0.7	-3 ± 2

^{a} CD$_3$CN solvent, ionic strength 0.07 M, values from 240 to 320 K. ^{b} μ_B. ^{c} K_{eq} = [low-spin]/[high-spin] (see text). ^{d} kcal mol^{-1}. ^{e} cal K^{-1} mol^{-1}. ^{f} Results for **Fe^{II}(D$_2$bip)-d_6** are the same within error. ^{g} Temperature range 250–320 K.

and ionic strength. The temperature dependence of the magnetic susceptibility was modeled assuming the high- and low-spin forms to have $\mu = 5.2$ and 0 μ_B, respectively (see Experimental Section). This yields $\Delta H° = -5.1 \pm 0.5$ kcal mol^{-1} and $\Delta S° = -21 \pm 2$ eu (Table 1), which are typical values for spin-equilibrium iron(II) complexes.[23,24]

Fe^{III}(H$_2$bip) in MeCN solution has a magnetic moment of 3.2 μ_B at 298 K, between that expected for low-spin (2.0 μ_B) and high-spin (5.9 μ_B) iron(III) complexes.[22] The variation in magnetic susceptibility from 249 to 322 K yields $\Delta H° = -2.8 \pm 0.3$ kcal mol^{-1} and $\Delta S° = -7 \pm 1$ eu for the spin equilibrium. In the UV−vis spectra of **Fe^{III}(H$_2$bip)** in MeCN, the band at 476 nm increases in intensity (ϵ) with increasing temperature, while the band at 504 nm decreases. Isosbestic points are observed at 380 and 490 nm, and the spectral changes are reversed upon cooling the sample back to its original temperature. The optical transition at 476 nm is due to the high-spin form, while the 504 nm band is due to the low-spin isomer. The ^{1}H NMR spectrum of **Fe^{III}(H$_2$bip)**, like the iron(II) derivative, consists of six resolved CH signals and an NH resonance, although two of the aliphatic resonances are extremely broad (>1000 Hz). All resonances broaden and shift as the temperature is increased from 280 to 350 K.

The deprotonated derivative **Fe^{III}(Hbip)** is readily prepared by exposure of **Fe^{II}(H$_2$bip)** to anhydrous oxygen either in solution or in the solid state. It appears to be NMR silent in CD$_3$CN. Its magnetic moment of 3.2 μ_B at 298 K is similar to

that of **Fe^{III}(H$_2$bip)** and is again indicative of a mixture of high- and low-spin forms (Table 1). The optical spectrum of **Fe^{III}-(Hbip)** is very similar to that of the biimidazoline analogue[12] with bands at 390 and 636 nm. The identity of **Fe^{III}(Hbip)** as a monodeprotonated complex was confirmed by reversible acid−base titration by UV−vis spectroscopy, reacting **Fe^{III}-(H$_2$bip)** with *N*-methylmorpholine followed by HClO$_4$.

[Co(H$_2$bim)$_3$](ClO$_4$)$_2$ [**Co^{II}(H$_2$bim)**] was prepared from [Co-(H$_2$O)$_6$](ClO$_4$)$_2$ following a modification of the procedure for the nitrate salt.[25] Its 4.5 μ_B magnetic moment in CD$_3$CN solution is substantially greater than the spin-only value, as is common for high-spin Co^{II} complexes.[22] The ^{1}H NMR spectrum shows three paramagnetically shifted signals. This is inconsistent with a static D_3 structure, which would have diastereotopic methylene hydrogens. The spectrum implies that a fluxional process is inverting the chirality at cobalt on the NMR time scale, as was suggested for **Fe^{II}(H$_2$bim)** on the same basis.[12]

[Co^{III}(H$_2$bim)$_3$](ClO$_4$)$_3$ [**Co^{III}(H$_2$bim)**] was synthesized by reacting the chloride salt of **Co^{II}(H$_2$bim)** with 3 equiv of AgClO$_4$. Treatment of **Co^{III}(H$_2$bim)** with a slight excess of LiN-^{i}Pr$_2$ gives [Co^{III}(Hbim)(H$_2$bim)$_2$](ClO$_4$)$_2$ [**Co^{III}(Hbim)**]. **Co^{III}-(H$_2$bim)** (1.8 mM) can also be deprotonated to **Co^{III}(Hbim)** with piperidine (>36 mM, 20 equiv) in MeCN, and back-titration with HClO$_4$/MeCN returns the starting material. Both of the Co(III) complexes exhibit sharp ^{1}H NMR spectra characteristic of diamagnetic, nonfluxional complexes. **Co^{II}-(H$_2$bim)** and **Co^{III}(H$_2$bim)** have been characterized by X-ray crystallography (Tables 2 and 3). Because the structures of the cations are very similar, only an ORTEP drawing of **Co^{III}-(H$_2$bim)** is included (Figure 2). Both complexes exhibit pseudo-octahedral geometry with ligand bite angles ranging from 74.6 (6)° in **Co^{II}(H$_2$bim)** to 81.6 (2)° in **Co^{III}(H$_2$bim)**. The smaller bite angles in the high-spin ion are the result of longer Co−N bonds. Co−N distances in low-spin **Co^{III}(H$_2$bim)** are 1.92 ± 0.02 Å for the three independent cobalt ions in the unit cell. In **Co^{II}(H$_2$bim)**, the Co−N distances vary from 2.089 (12) to 2.179 (13) Å. It is not apparent why the range is so large because the high-spin d^7 center is not expected to exhibit significant Jahn−Teller effects.[26] Although data were collected at 293 K for **Co^{II}-(H$_2$bim)** and at 161 K for **Co^{III}(H$_2$bim)**, the 0.17−0.26 Å contraction is typical of previously observed differences between high- and low-spin cobalt ions.[27] Hydrogen bonding interactions are indicated by close contacts between the perchlorate counterions and the amines, d(N⋯O) = 2.82 (1)−3.79 (3) Å.

II. Hydrogen-Atom Self-Exchange (Proton-Coupled Electron Transfer). A. Fe^{II}(H$_2$bip)/Fe^{III}(Hbip). The rate constant for net exchange of a hydrogen atom between **Fe^{II}(H$_2$bip)** and **Fe^{III}(Hbip)** was measured by ^{1}H NMR line broadening, analogous to studies of the iron biimidazoline system.[12] All six CH signals for **Fe^{II}(H$_2$bip)** in the ^{1}H NMR spectrum of **Fe^{II}-(H$_2$bip)** broaden upon addition of varying concentrations of NMR-silent **Fe^{III}(Hbip)** (Figure 3A). The chemical shifts remain constant over the concentration range examined, indicating that the system is in the slow exchange limit. In this limit, the change in line width ΔW gives the pseudo-first-order rate constant (k_{obs}

(23) (a) Reeder, K. A.; Dose, E. V.; Wilson, L. J. *Inorg. Chem.* **1978**, *17*, 1071−1075. (b) Dose, E. V.; Hoselton, M. A.; Sutin, N.; Tweedle, M. F.; Wilson, L. J. *J. Am. Chem. Soc.* **1978**, *100*, 1141−1147. (c) Jesson, J. P.; Trofimenko, S.; Eaton, D. R. *J. Am. Chem. Soc.* **1967**, *89*, 3158−3164.
(24) (a) Turner, J. W.; Schultz, F. A. *Inorg. Chem.* **1999**, *38*, 358−364. (b) Turner, J. W.; Schultz, F. A. *Inorg. Chem.* **2001**, *40*, 5296−5298. (c) Turner, J. W.; Schultz, F. A. *J. Phys. Chem. B* **2002**, *106*, 2009−2017.

(25) Wang, J. C.; Bauman, J. E., Jr. *Inorg. Chem.* **1965**, *4*, 1613.
(26) A reviewer has suggested that solid [Co^{II}(H$_2$bim)$_3$](ClO$_4$)$_2$ might contain some low-spin form, which would be expected to exhibit a Jahn−Teller distortion.
(27) Brunschwig, B. S.; Creutz, C.; Macartney, D. H.; Sham, T.-K.; Sutin, N. *Faraday Discuss. Chem. Soc.* **1982**, *74*, 113.

Table 2. Crystal Data and Structure Refinement for **Co^{II}(H₂bim)** and **Co^{III}(H₂bim)**[a]

compound	Co^{II}(H₂bim)	Co^{III}(H₂bim)·¹/₃CH₃CN
empirical formula	$C_{18}H_{30}Cl_2CoN_{12}O_8$	$C_{18.67}H_{31}Cl_3CoN_{12.33}O_{12}$
formula weight (g mol⁻¹)	672.37	785.50
crystal size (mm)	$0.48 \times 0.30 \times 0.24$	$0.13 \times 0.10 \times 0.05$
color	orange	red
volume (Å³)	2751.6(4)	4608.3(2)
density, calculated (Mg/m³)	1.623	1.698
temperature (K)	293(2)	161(2)
habit	monoclinic	triclinic
space group	Cc	$P\bar{1}$
unit cell dimensions (Å, deg)	$a = 13.3160(10)$	$a = 12.923(3)$ Å
	$b = 13.5443(12)$	$b = 19.835(6)$ Å
	$c = 16.0850(13)$	$c = 21.281(6)$ Å
	$\beta = 108.467(5)$	$\alpha = 113.596(14)°$
		$\beta = 97.895(14)°$
		$\gamma = 106.095(12)°$
Z	4	6
absorption coefficient (mm⁻¹)	0.885	0.900
θ range (deg)	3.01–20.80	2.05–20.84
index ranges	$-13 \leq h \leq 13$	$-12 \leq h \leq 12$
	$-12 \leq k \leq 13$	$-19 \leq k \leq 19$
	$-16 \leq l \leq 16$	$-21 \leq l \leq 21$
reflections/unique	2850/2850	19 630/9662
R (merge)	NA	0.0589
data/restraints/ parameters	2850/0/369	9662/0/1270
goodness-of-fit on F^2	1.094	0.995
R indices ($I > 2\sigma(I)$)[b]	$R_1 = 0.055$,	$R_1 = 0.048$,
	$wR_2 = 0.129$	$wR_2 = 0.117$
R indices (all data)	$R_1 = 0.079$,	$R_1 = 0.082$,
	$wR_2 = 0.152$	$wR_2 = 0.134$

[a] Data were collected on a Nonius Kappa CCD diffractometer using Mo Kα radiation ($\lambda = 0.7107$ Å). [b] $w = 1/[s^2(F_o^2) + (0.0759P)^2]$, where $P = (F_o^2 + 2F_c^2)/3$.

$= \pi\Delta W$), and the self-exchange rate constant is the dependence of the line broadening on **Fe^{III}(Hbip)** concentration (eq 6).[28] The full widths at half maximum (fwhm) of the **Fe^{II}(H₂bip)**

$$k_{Fe,H\bullet} = \frac{\pi(\Delta W)}{[Fe^{III}(H_2bip)]} \qquad (6)$$

resonances at δ 11 and -3 were used to determine the self-exchange rate constant $k_{Fe,H\bullet}$, because these are well separated from other signals. A plot of $\pi\Delta W$ versus [**Fe^{III}(Hbip)**] from a representative data set is shown in Figure 4. The line broadening was independent of the concentration of **Fe^{II}(H₂bip)** from 13 to 31 mM. Other ¹H NMR signals in the solution, such as those for CD₂HCN, did not broaden significantly upon addition of **Fe^{III}(Hbip)**.

The kinetics of H-atom self-exchange were examined by three individuals using samples from different batches of iron complexes and different lots of CD₃CN over a period of more than 1 year. All rate constants at 298 K fall within the estimated errors of ±20%, and their average is $k_{Fe,H\bullet} = (1.1 \pm 0.2) \times 10^4$ M⁻¹ s⁻¹ at 298 K. Changes in ionic strength between 80 and 156 mM by addition of ⁿBu₄NClO₄ did not affect the observed rate constant. Studies with compounds deuterated at the amine

(28) Sandström, J. *Dynamic NMR Spectroscopy*; Academic Press: New York, 1982.

**Table 3.** Bond Lengths (Å) and Angles (deg) for **Co^{II}(H₂bim)** and **Co^{III}(H₂bim)**

|	Co^{II}(H₂bim)	Co^{III}(H₂bim)
Co–N(1)	2.120(18)	1.937(5)
Co–N(3)	2.117(13)	1.909(5)
Co–N(5)	2.089(12)	1.927(6)
Co–N(7)	2.162(15)	1.929(5)
Co–N(9)	2.153(13)	1.909(5)
Co–N(11)	2.179(13)	1.938(5)
N(1)–Co–N(3)	74.6(6)	80.9(2)
N(1)–Co–N(5)	92.6(5)	91.6(2)
N(1)–Co–N(7)	94.7(6)	92.6(2)
N(1)–Co–N(9)	97.8(5)	94.3(2)
N(1)–Co–N(11)	171.9(4)	173.8(2)
N(3)–Co–N(5)	98.7(5)	93.9(2)
N(3)–Co–N(7)	168.4(6)	172.1(2)
N(3)–Co–N(9)	87.5(2)	92.1(2)
N(3)–Co–N(11)	98.0(5)	94.9(2)
N(5)–Co–N(7)	77.2(3)	81.6(2)
N(5)–Co–N(9)	169.0(5)	172.1(2)
N(5)–Co–N(11)	91.8(5)	93.2(2)
N(7)–Co–N(9)	98.4(6)	92.9(2)
N(7)–Co–N(11)	93.0(5)	91.9(2)
N(9)–Co–N(11)	78.3(4)	81.3(2)
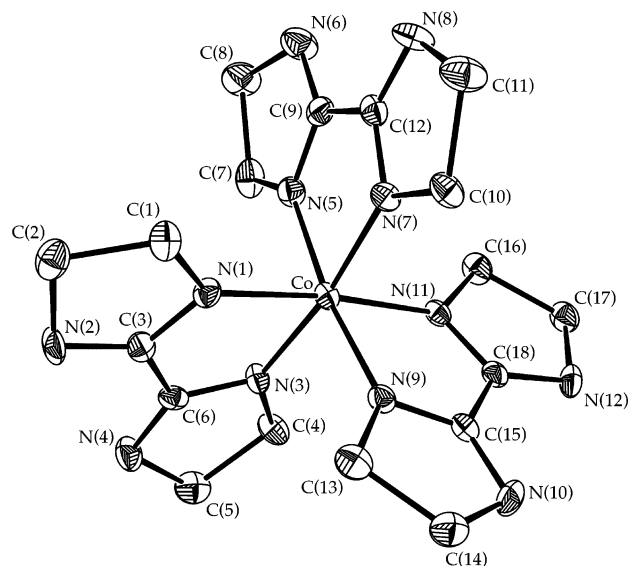
Figure 2. ORTEP representation of the cation in the solid-state structure of [Co(H₂bim)₃](ClO₄)₃ (**Co^{III}(H₂bim)**). Ellipsoids are drawn at 30%, and hydrogen atoms were removed for clarity. The same numbering scheme is used for the structure of **Co^{II}(H₂bim)**.

positions, **Fe^{II}(D₂bip)-d₆** and **Fe^{III}(Dbip)-d₅**, showed an isotope effect of 1.6 ± 0.5 at 298 K. This is close to the value of 2.3 ± 0.3 at 324 K found for high-spin iron biimidazoline complexes.[12]

Three separate experiments were run to measure the temperature dependence of the H-atom self-exchange rate constant. The values agree within the 20% error bars (±0.18 ln units), but the two later data sets have systematically slower rates than the earlier set (Figure 5). We have not been able to determine the reason(s) for this difference. Within each of the data sets, the rate constants *decrease* with increasing temperature. Each experiment has been fit by the Eyring equation, which we feel is more valid than fitting all three experiments together, given the small but significant systematic errors. Negative activation energies are observed in each case, -1.1, -1.5, and -1.9 kcal mol⁻¹ (estimated errors ±0.5 kcal mol⁻¹), and all three have unusually large entropies of activation (-44, -45, and -46
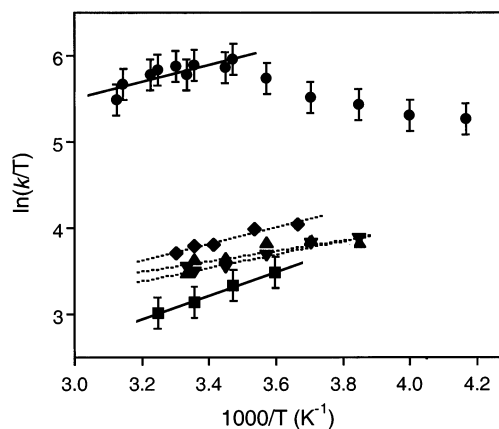
A. (H•)

B. (e⁻)
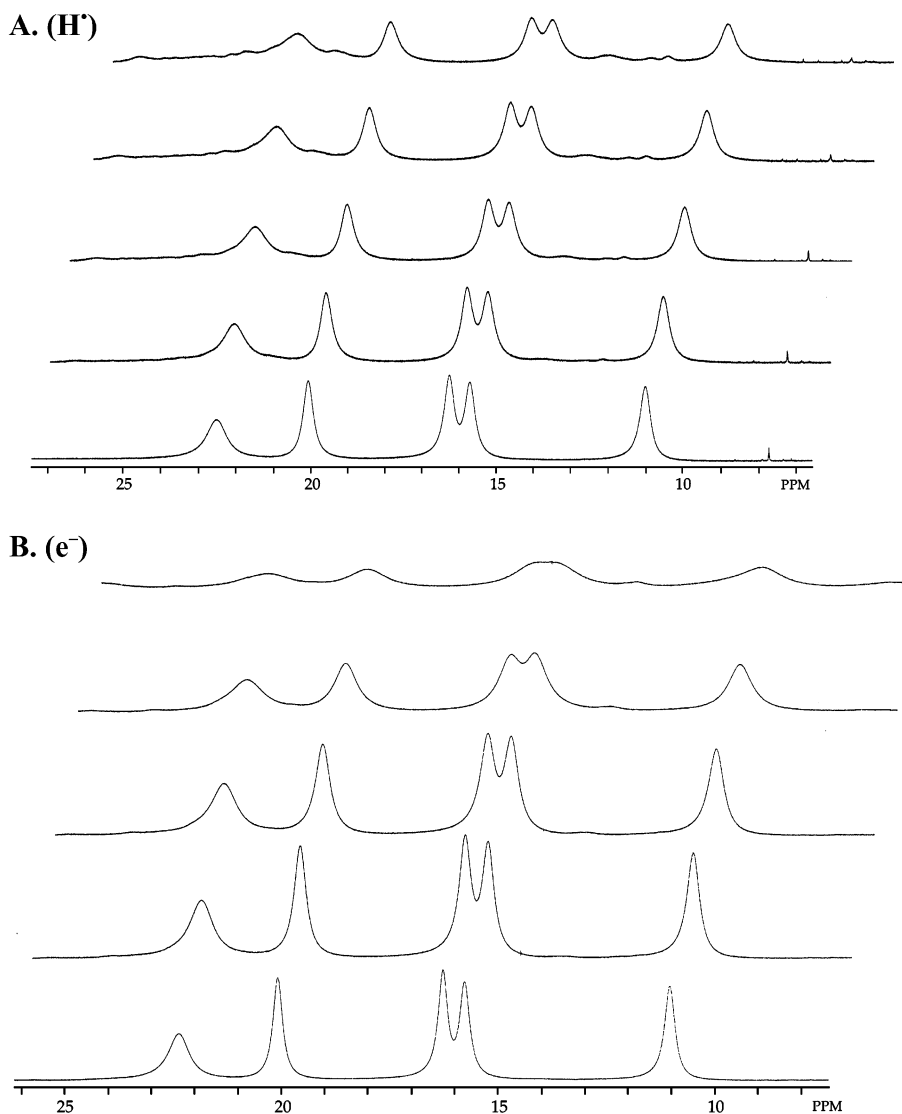
Figure 3. Portions of 500 MHz ^{1}H NMR spectra for **Fe^{II}(H$_2$bip)** recorded in the presence of increasing amounts of **Fe^{III}(Hbip)** (A, top) or **Fe^{III}(H$_2$bip)** (B, bottom) in CD$_3$CN. The spectra are offset; line broadening occurs without significant shifting of peak positions.
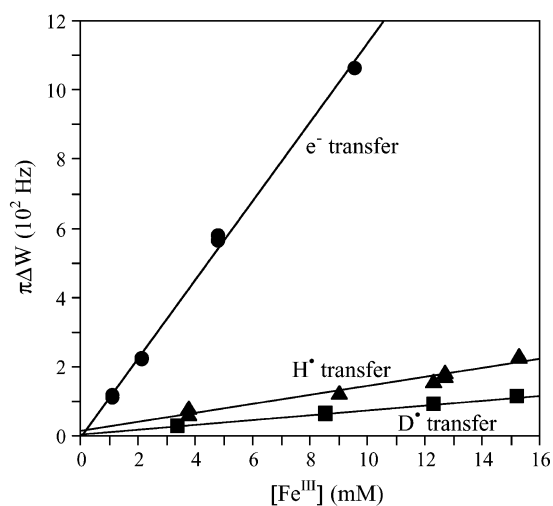
**Figure 4.** A plot of line broadening ($\pi\Delta W$) for resonances of **Fe^{II}(H$_2$bip)** (or **Fe^{II}(D$_2$bip)-d_6** for ■) versus the concentration of **Fe^{III}(H$_2$bip)** (●), **Fe^{III}(Hbip)** (▲), or **Fe^{II}(Dbip)-d_5** (■).

Figure 5. Eyring plots of self-exchange rate constants for electron (●), hydrogen atom (◆, ▲, ▼), and deuterium atom transfer (■) between iron 2,2′-bi-(tetrahydro)pyrimidine complexes. Three H-atom self-exchange experiments are shown and separately fit to the Eyring equation (dashed lines); see text. Error bars are not shown on the H-atom lines for clarity.

eu). We therefore assign the activation parameters for H-atom self-exchange as $\Delta H^{\ddagger} = -1.5 \pm 0.5$ kcal 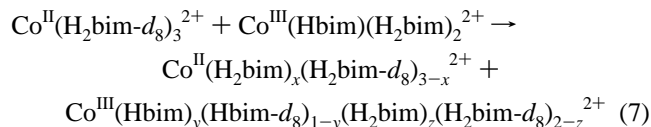mol^{-1} and $\Delta S^{\ddagger} =$ -45 ± 5 (H) eu. Deuterium-atom self-exchange between N-deuterated derivatives shows an even more negative $\Delta H^{\ddagger}$ of -2.7 ± 0.5 kcal mol^{-1} and $\Delta S^{\ddagger} = -50 \pm 5$ eu.
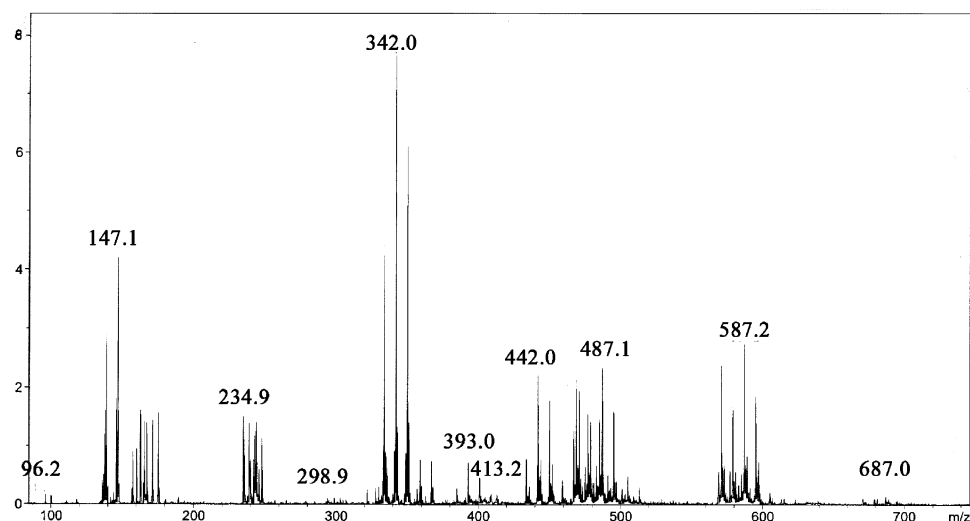
Figure 6. Detail of the electrospray mass spectrum of a mixture of [Co^{II}(H$_2$bim-d_8)$_3$](ClO$_4$)$_2$ and [Co^{III}(Hbim)(H$_2$bim)$_2$](ClO$_4$)$_2$ in MeCN solution indicating exchange of biimidazoline ligands between metal centers.

B. Co^{II}(H$_2$bim)/Co^{III}(Hbim). Hydrogen-atom transfer reactions of the cobalt derivatives **Co^{II}(H$_2$bim)** and **Co^{III}(Hbim)** with hydroxylamines and stable oxygen radicals are much slower than those of the iron derivatives at similar driving forces.[8] This was attributed to a large intrinsic barrier for hydrogen-atom exchange.[8] To probe reactions on a slow time scale, **Co^{III}(Hbim)** was reacted with **Co^{II}(H$_2$bim)-d_{24}**, deuterated at the aliphatic positions. Contrary to expectations, chemical exchange of the deuterium label was complete upon acquiring the first ^{1}H and ^{2}H NMR spectra, in both CD$_3$CN and DMSO-d_6. A second-order rate constant $k \geq 1$ M^{-1} s^{-1} can be estimated from this result.

Electrospray ionization mass spectrometry (ESI-MS) of separate solutions of **Co^{II}(H$_2$bim)-d_{24}** and **Co^{III}(Hbim)** show distinct patterns, with a major peak for **Co^{II}(H$_2$bim)-d_{24}** at m/z = 450 ([Co(H$_2$bim-d_8)$_2$(ClO$_4$)]$^+$), and for **Co^{III}(Hbim)** at m/z = 471 ([Co(Hbim)$_2$(H$_2$bim)]$^+$). ESI-MS of a reaction containing equimolar amounts of **Co^{II}(H$_2$bim)-d_{24}** and unlabeled **Co^{III}-(Hbim)**, after 30 min of stirring in MeCN, showed that ligand exchange had occurred (Figure 6). For both species, mass clusters were observed corresponding to successive exchanges of H$_2$bim and H$_2$bim-d_8, a change of 8 mass units per exchange (eq 7). Ligand exchange is slow for the low-spin d^6 cobalt(III) complexes **Co^{III}(Hbim)** and **Co^{III}(H$_2$bim)** in the absence of **Co^{II}(H$_2$bim)**. Although the low solubility of biimidazoline precludes exchange studies using H$_2$bim-d_8, the reaction of excess H$_2$bip with **Co^{III}(Hbim)** in acetonitrile solution showed only partial ligand substitution after 1 day.

$$\text{Co}^{II}(\text{H}_2\text{bim-}d_8)_3^{2+} + \text{Co}^{III}(\text{Hbim})(\text{H}_2\text{bim})_2^{2+} \rightarrow$$
$$\text{Co}^{II}(\text{H}_2\text{bim})_x(\text{H}_2\text{bim-}d_8)_{3-x}^{2+} +$$
$$\text{Co}^{III}(\text{Hbim})_y(\text{Hbim-}d_8)_{1-y}(\text{H}_2\text{bim})_z(\text{H}_2\text{bim-}d_8)_{2-z}^{2+} \quad (7)$$

^{1}H NMR spectra of solutions containing unlabeled **Co^{II}-(H$_2$bim)** and **Co^{III}(Hbim)** in DMSO-d_6 are significantly broadened. At >0.1 M **Co^{II}(H$_2$bim)**, the aliphatic resonances for **Co^{III}(Hbim)** are extremely broad and approach coalescence. Analysis of the line widths for the aliphatic resonances of **Co^{III}-(Hbim)** at various concentrations of **Co^{II}(H$_2$bim)** as above gives $k = (5.8 \pm 0.5) \times 10^3$ M^{-1} s^{-1}. Similar experiments in CD$_3$-

CN precipitate dark green-brown solids after 10−15 min. Addition of HClO$_4$ causes dissolution of the solids and appearance of ^{1}H NMR signals for only **Co^{II}(H$_2$bim)** and **Co^{III}-(H$_2$bim)** in 95 ± 5% yields.

The data indicate that rapid exchange between **Co^{II}(H$_2$bim)-d_{24}** and **Co^{III}(Hbim)** occurs via an inner-sphere mechanism with transfer of an Hbim ligand. Most likely, the deprotonated nitrogen on **Co^{III}(Hbim)** serves as a ligand for the substitution labile cobalt(II) center. Such an association is supported by the precipitation of **Co^{II}(H$_2$bim)/Co^{III}(Hbim)** solids from acetonitrile. Consistent with this proposal, reactions of **Co^{II}(H$_2$bim)** with **Fe^{III}(Hbim)** or **Fe^{III}(Hbip)** form multiple species (by optical spectroscopy).

III. Electron Self-Exchange. A. Fe^{II}(H$_2$bip)/Fe^{III}(H$_2$bip). ^{1}H NMR line broadening was used to determine the rate constant for exchange of an electron between **Fe^{II}(H$_2$bip)** and **Fe^{III}-(H$_2$bip)**, following the procedure above (Figures 3B, 4). Again, all six CH signals for **Fe^{II}(H$_2$bip)** broaden while their chemical shifts remain constant over the concentration range examined, indicating that the system is in the slow exchange limit. **Fe^{III}-(H$_2$bip)** exhibits a very broad ^{1}H NMR spectrum in the 10−25 ppm region, but the small overlap of some of these resonances with those for **Fe^{II}(H$_2$bip)** does not appear to affect the measurements. As found for the H-atom exchange, the line broadening was independent of the concentration of **Fe^{II}(H$_2$bip)**, other ^{1}H NMR signals from the solution did not broaden significantly on addition of **Fe^{III}(H$_2$bip)**, and there was no dependence on ionic strength between 80 and 160 mM (^{n}Bu$_4$-NClO$_4$). The derived second-order rate constant, $k_{\text{Fe,e}-}$, is (1.1 ± 0.2) × 10^5 M^{-1} s^{-1} (298 K in CD$_3$CN, μ = 74−100 mM).

Rate constants for electron self-exchange *decrease* on raising the temperature from 288 to 320 K, as observed for H-atom self-exchange (Figure 5, Table 4). Surprisingly, the rate constants also decrease on lowering the temperature from 288 to 240 K. Thus, the maximum rate of self-exchange is observed at 288 K. Fitting the rate constants from 288 to 320 K to the Eyring equation gives parameters similar to the H-atom case (Table 4), with a negative enthalpy of activation and a large negative entropy of activation: $\Delta H^{\ddagger} = -2.1 \pm 0.5$ kcal mol^{-1} and $\Delta S^{\ddagger} = -42 \pm 5$ eu. Fitting the lower temperature data
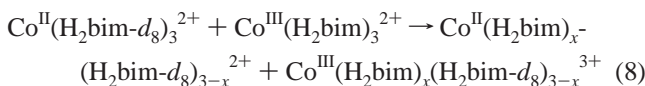
Table 4. Hydrogen-Atom and Electron Self-Exchange Rate Constants[a]

reaction	self-exchange	k (M^{-1} s^{-1})[b]	$\Delta G^{\ddagger}$ [c,d]	$\Delta H^{\ddagger}$ [d]	$\Delta S^{\ddagger}$ [e]
Fe^{II}(H$_2$bip) + Fe^{III}(Hbip)	H-atom	$(1.1 \pm 0.2) \times 10^4$	11.9 ± 0.1	-1.5 ± 0.5[f]	-45 ± 5[f]
Fe^{II}(D$_2$bip) + Fe^{III}(Dbip)	D-atom	$(6.8 \pm 1.0) \times 10^3$	12.2 ± 0.1	-2.7 ± 0.5	-50 ± 5
Fe^{II}(H$_2$bim) + Fe^{III}(Hbim)	H-atom	$(5.8 \pm 0.9) \times 10^3$	12.3 ± 0.1	4.4 ± 0.7	-26 ± 2
Fe^{II}(H$_2$bip) + Fe^{III}(H$_2$bip)	electron	$(1.1 \pm 0.2) \times 10^5$	10.6 ± 0.1	$[-2.1 \pm 0.5]$[g]	$[-42 \pm 5]$[g]
Fe^{II}(H$_2$bim) + Fe^{III}(H$_2$bim)	electron	$(1.7 \pm 0.2) \times 10^4$	11.7 ± 0.1	4.1 ± 0.3	-25 ± 1
Co^{II}(H$_2$bim) + Co^{III}(H$_2$bim)[d]	electron	$\lesssim 10^{-7}$ [h]	$\gtrsim 27$		
Co^{II}(H$_2$bim) + Co^{III}(Hbim)[d]	H-atom	$10^{-3} - 10^{-9}$ [i]	26 ± 4		

[a] In CD$_3$CN solvent, 298 K. Data for H$_2$bim reactions from ref 12. [b] Estimated errors ±20%. [c] At 298 K. [d] kcal mol^{-1}. [e] cal K^{-1} mol^{-1}. [f] Average of activation parameters from three separate experiments; see text. [g] From rate constants at 288–320 K; rate constants 240–288 K give $\Delta H^{\ddagger} = +1.9 \pm 0.5$ kcal mol^{-1} and $\Delta S^{\ddagger} = -29 \pm 3$ eu. [h] Estimated using the Marcus cross relation from the rate of electron transfer from **Co^{II}(H$_2$bim)** to **Fe^{III}(H$_2$bim)**. [i] Table 5.

(240–288 K) gives more normal values: $\Delta H^{\ddagger} = +1.9 \pm 0.5$ kcal mol^{-1} and $\Delta S^{\ddagger} = -29 \pm 3$ eu.

B. Co^{II}(H$_2$bim)/Co^{III}(H$_2$bim). As in the hydrogen-atom self-exchange studies above, deuterium scrambling between **Co^{II}-(H$_2$bim)-d_{24}** and **Co^{III}(H$_2$bim)** in CD$_3$CN is essentially complete upon acquisition of the first ^{1}H or ^{2}H NMR spectrum ($k > 10^{-1}$ M^{-1} s^{-1}). ESI-MS analysis showed that scrambling of ligands had occurred (eq 8). For instance, mass clusters were observed at 671, 679, 687, and 695 daltons for the d_0, d_8, d_{16}, and d_{24} isotopomers of [Co(H$_2$bim)$_3$(ClO$_4$)$_2$]$^+$. This ion is not observed

$$\text{Co}^{\text{II}}(\text{H}_2\text{bim-}d_8)_3{}^{2+} + \text{Co}^{\text{III}}(\text{H}_2\text{bim})_3{}^{2+} \rightarrow \text{Co}^{\text{II}}(\text{H}_2\text{bim})_x\text{-}$$
$$(\text{H}_2\text{bim-}d_8)_{3-x}{}^{2+} + \text{Co}^{\text{III}}(\text{H}_2\text{bim})_x(\text{H}_2\text{bim-}d_8)_{3-x}{}^{3+} \quad (8)$$

in spectra of **Co^{III}(Hbim)** or **Co^{II}(H$_2$bim)**. The ligand scrambling indicates an inner-sphere process, as found for the H-atom transfer above, but the absence of a basic, deprotonated nitrogen in the oxidant may indicate a different mechanism. No broadening of the ^{1}H NMR resonances for **Co^{III}(H$_2$bim)** is observed in the presence of **Co^{II}(H$_2$bim)** ($k < 10^2$ M^{-1} s^{-1}), in contrast to H-atom transfer reactions containing **Co^{III}(Hbim)** and **Co^{II}-(H$_2$bim)**.

The Co^{II}/Co^{III} electron self-exchange rate was determined by an alternative procedure, using the Marcus cross relation (eq 1). The rate of electron transfer between **Co^{II}(H$_2$bim)** and **Fe^{III}-(H$_2$bim)** was determined by stopped-flow UV–vis spectroscopy under pseudo-first-order conditions using **Co^{II}(H$_2$bim)** in excess at various concentrations. First-order decay of **Fe^{III}(H$_2$bim)** was observed for two half-lives. The rate constant $k_{\text{CoFe}} = 50 \pm 15$ M^{-1} s^{-1} was obtained (the uncertainty arising in part from the slow oxidation of **Fe^{II}(H$_2$bim)** by adventitious O$_2$). The other parameters needed for the cross relation are (i) electron-transfer self-exchange between **Fe^{II}(H$_2$bim)** and **Fe^{III}(H$_2$bim)**, $k_{\text{FeFe}} = (1.7 \pm 0.2) \times 10^4$ M^{-1} s^{-1},[12] and (ii) the equilibrium constant $K_{\text{CoFe}} \cong 8 \times 10^4$ (from the reduction potentials: -0.31 ± 0.05 V for **Fe^{II}(H$_2$bim)**[17] and -0.6 ± 0.1 V for **Co^{III}(H$_2$bim)**[8,29] in MeCN vs Cp$_2$Fe$^{+/o}$). These values yield 10^{-6} M^{-1} s^{-1} for the electron-transfer self-exchange rate constant between **Co^{II}-(H$_2$bim)** and **Co^{III}(H$_2$bim)**. This calculation assumes that reaction of **Co^{II}(H$_2$bim)** + **Fe^{III}(H$_2$bim)** proceeds by outer-sphere electron transfer. Because it is possible that the reaction proceeds by an inner-sphere path, 10^{-6} M^{-1} s^{-1} is an upper limit to the rate constant for outer-sphere electron transfer.

Discussion

I. Self-Exchange Reactions Involving Iron Complexes. The H$_2$bip and H$_2$bim ligands used here differ only in that the former

has one more methylene group in each ring. This difference is sufficient to have the iron-H$_2$bip complexes be mixtures of high-spin and low-spin forms at 298 K in MeCN solution, while the H$_2$bim analogues are high-spin at this temperature.[12] In addition, racemization of **Fe^{II}(H$_2$bip)** is slow on the NMR time scale (D_3 symmetry), while **Fe^{II}(H$_2$bim)** is highly fluxional (apparent D_{3h} symmetry) even at 235 K in MeCN.[12] Self-exchange rate constants have been determined both for electron transfer and for transfer of both an electron and a proton. We call the latter hydrogen-atom transfer, but it could equally well be called proton-coupled electron transfer because the proton and electron are transferred between different sites in a single kinetic step. The H$_2$bip complexes undergo self-exchange slightly faster than the H$_2$bim analogues: 1.9 times faster for H-atom transfer and 6.5 times faster for electron transfer at 298 K (Table 4). The isotope effects for H- versus D-atom exchange are similar: 1.6 ± 0.5 (H$_2$bip, 298 K) and 2.3 ± 0.3 (H$_2$bim, 324 K). Given the differences in the magnetic and spectroscopic properties of the compounds, it is perhaps surprising that the differences are not larger.

The most striking feature of the H$_2$bip electron and atom self-exchanges is that the reactions exhibit *negative* activation enthalpies, $\Delta H^{\ddagger} = -1.5$ (H$^{\bullet}$), -2.7 (D$^{\bullet}$), and -2.1 (e$^-$) kcal mol^{-1}, in the temperature range around room temperature. While this manuscript was under review, the only other example of an electron self-exchange reaction with $\Delta H^{\ddagger} < 0$ was reported.[30] Negative activation enthalpies are not common for any class of reaction but have been observed in a number of cases.[31] One explanation is that for endoergic reactions ($\Delta G > 0$) with favorable enthalpies, $\Delta H < 0$ and $\Delta S \ll 0$, the activation energy can be negative because the transition state resembles the products.[32–34] This does not apply to self-exchange reactions, for which $\Delta G = \Delta H = \Delta S = 0$. The more typical explanation for reactions that have $\Delta H^{\ddagger} < 0$ — the one that likely applies here and that was invoked in the recent report[30] — is that they

(29) Yoder, J. C.; Roth, J. P.; Won, T. J.; Mayer, J. M., work in progress.

(30) Fukuzumi, S.; Endo, Y.; Imahori, H. *J. Am. Chem. Soc.* **2002**, *124*, 10974–5.

(31) (a) A recent paper provides an excellent overview and leading references: Frank, R.; Greiner, G.; Rau, H. *Phys. Chem. Chem. Phys.* **1999**, *1*, 3481–3490. See also: (b) Braddock, J. N.; Meyer, T. J. *J. Am. Chem. Soc.* **1973**, *95*, 3158–3162. (c) Cramer, J. L.; Meyer, T. J. *Inorg. Chem.* **1974**, *13*, 1250–2. (d) Marcus, R. A.; Sutin, N. *Inorg. Chem.* **1975**, *14*, 213–6. (e) Montejano, H. A.; Avila, V.; Garrera, H. A.; Previtali, C. M. *J. Photochem. Photobiol. A-Chem.* **1993**, *72*, 117–122. (f) Kirowaeisner, E.; Schwarz, M.; Rosenblum, M.; Gileadi, E. *J. Electrochem. Soc.* **1994**, *141*, 1183–1190. (g) Sun, H.; Yoshimura, A.; Hoffman, M. Z. *J. Phys. Chem.* **1994**, *98*, 5058–5064. (h) Kapinus, E. I.; Rau, H. *J. Phys. Chem. A* **1998**, *102*, 5569–5576. (i) Fukuzumi, S.; Ohkubo, K.; Tokuda, Y.; Suenobu, T. *J. Am. Chem. Soc.* **2000**, *122*, 4286–4294.
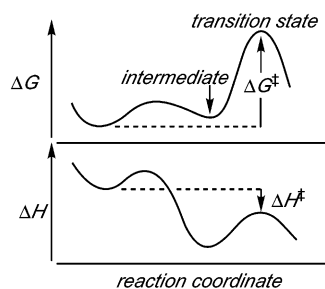
(32) $\Delta H^{\ddagger} < 0$ can also occur for reactions with $\Delta G = 0$ when $\Delta S \ll 0$.[31a,d]

(33) A more general derivation for electron-transfer reactions is given in ref 31d.

(34) For example: Brown, S. N.; Mayer, J. M. *J. Am. Chem. Soc.* **1996**, *118*, 12119–12133.

Figure 7. Schematic free energy and enthalpy surfaces for a reaction with a preequilibrium step and $\Delta H^\ddagger < 0$.

Figure 8. Measured ($\blacklozenge$) and model ($-$) electron self-exchange rate constants (left axis). $k(\text{model}) = \chi(\text{Fe}^{II}\text{H}_2\text{bip}) \times \chi(\text{Fe}^{III}\text{H}_2\text{bip}) \times k(\text{low-spin self-exchange})$ [k_{LS}, $\cdots$] (see text). Mole fractions of the low-spin forms are also shown (right axis): $\chi(\text{Fe}^{II})$ (- - -), $\chi(\text{Fe}^{III})$ ($--$).

proceed via an enthalpically favorable preequilibrium step.[31] As illustrated in Figure 7, when the $\Delta H_1°$ for the preequilibrium step is large and negative, and the following step has a small activation enthalpy $\Delta H_2^\ddagger$, then the overall $\Delta H^\ddagger = \Delta H_1° + \Delta H_2^\ddagger$ will be negative.[31]

The preequilibrium step is probably not the formation of the precursor complex prior to electron transfer or hydrogen-atom transfer/PCET. The iron complexes are all cationic, so precursor complex formation should have $\Delta H° > 0$ for electrostatic reasons.[1d,35] The formation of some favorable cation/perchlorate cluster seems ruled out by the lack of a dependence on $^n\text{Bu}_4$-NClO_4 concentration. Also, one would expect the precursor complex for H-atom transfer to have an $\text{N-H}\cdots\text{N}$ hydrogen bond and therefore be different from the precursor complex for electron transfer, yet the $\Delta H^\ddagger$ values for the two processes are similar.

The likely explanation is that isomerization of one or both of the iron bipyrimidine complexes from high-spin (HS) to low-spin (LS) precedes the chemical exchange reaction. HS to LS conversions have negative $\Delta H°$ values from -1.9 to -5.1 kcal mol^{-1} (Table 1). When electron and H-atom transfer occur preferentially between low-spin ions, the rates can slow with increasing temperature because less of the low-spin forms are present. This explanation is adapted from Turner and Shultz's argument that preequilibrium spin state changes occur in Fe^{II}/Fe^{III} and Co^{II}/Co^{III} electrochemical interconversions $-$ although in their case the high-spin form is the more reactive partner.[24]
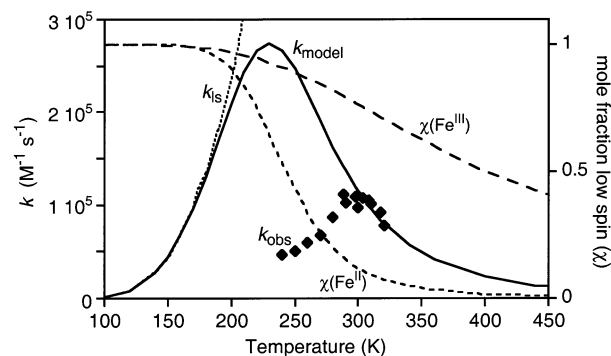
A simple model that qualitatively reproduces the data assumes that the self-exchange reactions involve only low-spin ions (eq 9; LS = low-spin; the asterisk identifies the different complexes). This is a major simplification of the reactions, because a complete description would include reactions that could occur

$$*\text{LS Fe}^{II} + \text{LS Fe}^{III} \xrightarrow{k_{LS}} *\text{LS Fe}^{III} + \text{LS Fe}^{II} \qquad (9)$$

not only between pairs of low-spin (LS) ions, but also between pairs of high-spin (HS) ions, between LS Fe^{II} and HS Fe^{III}, between HS Fe^{II} and LS Fe^{III}, and each of these could occur with or without spin change at either iron. Still, the assumption that reactions of the low-spin ions dominate is reasonable because in d^5/d^6 iron complexes electron self-exchange is often more facile for fully low-spin ions than for high-spin derivatives.[36] For instance, electron self-exchange is 1000 times faster for the low-spin 1,10-phenanthroline complexes [Fe(phen)$_3$]$^{2+/3+}$

(35) (a) Wherland, S. *Coord. Chem. Rev.* **1993**, *93*, 149. (b) There can, however, be a significant effect of the counterion (e.g., as in ref 37).

(36) Meyer, T. J.; Taube, H. Electron Transfer Reactions. *Comprehensive Coordination Chemistry*; Pergamon Press: New York, 1987; Vol. 1, Chapter 7.2.

(1.4×10^7 M^{-1} s^{-1} for the ClO$_4^-$ salt)[37] than for high-spin [Fe(H$_2$bim)$_3$]$^{2+/3+}$ (1.7×10^4 M^{-1} s^{-1}).[12] This is a result of smaller inner-sphere reorganization energies for the low-spin ions.

In the low-spin model, the rate constant k_{model} is the product of k_{LS} (eq 9) times the mole fractions of the LS iron(II) and LS iron(III) complexes $\chi_{LS}(\text{Fe}^{II})$ and $\chi_{LS}(\text{Fe}^{III})$ (eq 10). The mole fractions are derived from the equilibrium constants K_{II} and K_{III} as in eq 11. K_{II} and K_{III} have been measured independently from

$$k_{\text{model}} = \chi_{LS}(\text{Fe}^{II})\chi_{LS}(\text{Fe}^{III})k_{LS} \qquad (10)$$

$$\chi_{LS}(\text{Fe}^{II}) = \frac{K_{II}}{1 + K_{II}} \qquad K_{II} = \frac{[\text{LS}]}{[\text{HS}]} \qquad (11)$$

the magnetic susceptibility data (Table 1). HS/LS interconversion is treated as a rapid equilibrium because it is typically much faster than the millisecond NMR time scale involved here.[23] Because the low-spin forms are enthalpically favored, $\chi(\text{Fe}^{II})$ and $\chi(\text{Fe}^{III})$ vary from 1 at low temperatures toward zero at high temperatures, as shown in Figure 8 (dashed lines, right axis). As a crude approximation, k_{LS} at various temperatures is taken to be equal to the values reported for [Fe(phen)$_3$]$^{2+/3+}$ ($\Delta H^\ddagger = 2.0$ kcal mol^{-1} and $\Delta S^\ddagger = -19$ eu).[37]

A rough calculation for electron self-exchange between **Fe^{II}-(H$_2$bip)** and **Fe^{III}(H$_2$bip)** provides qualitative support for this model. At 298 K, k_{model} (4.4×10^5 M^{-1} s^{-1}) is a factor of 12 faster than the observed self-exchange rate constant, 1.1×10^5 M^{-1} s^{-1}. More importantly, the temperature dependence of the model shows the same negative activation energy as the data. This is shown in Figure 8, where the k_{model} has been divided by 12 to place it on the same scale as the data (dividing by 12 is the same as assuming that k_{LS} has an $\Delta S^\ddagger$ 5 eu larger than [Fe(phen)$_3$]$^{2+/3+}$). The model predicts a roughly parabolic dependence of rate constant on temperature, as observed. However, the quantitative agreement is poor as the model peaks at 230 K, some 60 K lower than the data. The discrepancy could in part be due to the use of [Fe(phen)$_3$]$^{2+/3+}$ for k_{LS}, but the position of the inflection point is due largely to the position of the spin-exchange equilibria. In the model, the low-temperature limit has $k_{\text{model}} = k_{LS}$ because the $K/(1 + K)$ terms approach 1. Thus, the observed low-temperature activation parameters

(37) Chan, M. S.; Wahl, A. C. *J. Phys. Chem.* **1978**, *82*, 2542−9. For [Fe(phen)$_3$]$^{2+,3+}$, $k = 13.6 \times 10^6$ M^{-1} s^{-1} for the ClO$_4^-$ salts and 6.0×10^6 M^{-1} s^{-1} for the PF$_6^-$ salts.

approach the activation parameters for the self-exchange step. The observed $\Delta H^{\ddagger}$ of 1.9 kcal mol^{-1} for the lower temperature data (Table 4) is reasonably typical of electron self-exchange of low-spin iron complexes.[36,37] At higher temperatures where $K_{II} \ll 1$, $k_{model} \cong K_{II}k_{LS}$ and $\Delta H^{\ddagger} \cong \Delta H_{II}{}^{\circ} + \Delta H_{LS}{}^{\ddagger}$ (neglecting the small variation in K_{III}). Because $\Delta H_{II}{}^{\circ} = -5$ kcal mol^{-1} and $\Delta H_{LS}{}^{\ddagger} \cong +2$ kcal mol^{-1}, the unusual negative enthalpies of activation are explained by this model, in which the reaction occurs predominantly between low-spin Fe^{II} and Fe^{III} complexes.

The isotope effect for hydrogen/deuterium-atom transfer also shows an interesting temperature dependence, suggesting substantial proton and deuteron tunneling. Tunneling has been proposed for a number of metal-mediated H-atom transfer/PCET reactions on the basis of unusually large isotope effects on rate constants.[38] Reactions that proceed primarily by tunneling can also show small values of k_H/k_D, such as the $k_H/k_D = 1.6 \pm 0.5$ at 298 K found here.[16,39] Semiclassically, isotope effects result from differences in zero-point energies and are therefore predominantly enthalpic, with $\Delta H^{\ddagger}(D) - \Delta H^{\ddagger}(H) = E_a{}^D - E_a{}^H > 0$ and Arrhenius preexponential factors about equal ($A^H/A^D \cong 1$).[40] When tunneling contributes to the reaction, Arrhenius plots should be curved. This curvature is typically not discernible over a small temperature range, but it leads to unusual activation parameters.[40,41] Apparent values of $E_a{}^D - E_a{}^H$ larger and A^H/A^D smaller than the semiclassical predictions are typically taken to indicate small or moderate tunneling corrections.[40] When the extent of tunneling is large, the situation is reversed.[40a] Reactions that proceed completely by tunneling from the ground state are temperature independent ($\Delta E_a = 0$), and $k_H/k_D = A^H/A^D$ is the ratio of the tunneling probabilities, normally $\gg 1$. The values observed here are $E_a{}^D - E_a{}^H = -1.2 \pm 0.8$ kcal mol^{-1} and $\log(A^H/A^D) = 0.9 \pm 1.2$ (Figure 5, Table 4). Although the error bars are large, the values suggest a predominantly tunneling mechanism.[42] This would appear to be consistent with the theoretical analysis of **Fe(H$_2$bim)**-**Fe(Hbim)** H-atom self-exchange by Hammes-Schiffer et al.[16c] The importance of tunneling is particularly evident in the unusual negative $E_a{}^D - E_a{}^H$, opposite in sign from that predicted by a semiclassical zero-point energy treatment.

The discussion above assumes that **Fe^{II}(H$_2$bip)**/**Fe^{III}(Hbip)** self-exchange occurs by one-step H-atom or proton-coupled electron transfer (PCET), analogous to **Fe^{II}(H$_2$bim)** + **Fe^{III}-(Hbim)**. In the H$_2$bim system, stepwise mechanisms were ruled out on the basis of the primary isotope effect (eliminating rate-limiting electron transfer) and the fact that initial electron or

proton transfer is ~ 0.5 V (11.5 kcal mol^{-1}) uphill.[12] Initial e$^-$ or H$^+$ transfer from **Fe^{II}(H$_2$bip)** to **Fe^{III}(Hbip)** is apparently uphill by only ~ 0.14 V (3.2 kcal mol^{-1}) based on preliminary electrochemical experiments.[43] Therefore, the data do not rule out alternative mechanisms of (i) initial, rate-limiting proton transfer followed by electron transfer, or (ii) preequilibrium electron transfer followed by proton transfer (which are the microscopic reverse of each other[12]). However, similar mechanisms are suggested for the H$_2$bip and H$_2$bim systems by their similar rate constants (Table 4) and by that both values have been successfully used as H-atom self-exchange rate constants in our application of the cross relation to H-atom transfer.[8] It would be difficult to rationalize the negative activation energies with a preequilibrium electron or proton transfer that is endothermic.

II. Self-Exchange Reactions Involving Cobalt Complexes. These reactions interconvert high-spin **Co^{II}(H$_2$bim)** and low-spin **Co^{III}(Hbim)** or **Co^{III}(H$_2$bim)**. Co^{II}/Co^{III} redox reactions that involve such spin state changes are typically very slow, with electron self-exchange rate constants often on the order of 10^{-4} to 10^{-6} M^{-1} s^{-1}.[36] The slow rate constants for these reactions are often attributed not to the spin state change itself, but to the associated large changes in cobalt−ligand bond lengths, which result in a high inner-sphere reorganization energy.[1c,18,44] However, it has also been suggested that these reactions are slow because they proceed by preequilibrium isomerization to high-spin Co^{III} [24] or because the spin state change requires quantum mechanical mixing of ground and excited states.[45] The Co−N bond lengths are ~ 0.2 Å shorter in **Co^{III}(H$_2$bim)** than in **Co^{II}(H$_2$bim)**. This is a significant difference, as the value for the iron analogues is ~ 0.1 Å[12] and inner-sphere reorganization energies vary as the square of the displacement.[1] By analogy with related cobalt systems,[36] the 0.2 Å change in Co−N bond lengths would predict very slow electron self-exchange, consistent with the 10^{-6} M^{-1} s^{-1} value determined using the Marcus cross relation.

Hydrogen-atom self-exchange between **Co^{II}(H$_2$bim)** and **Co^{III}(Hbim)** also involves interconversion of high- and low-spin complexes presumably also with a large change in Co−N bond lengths. Thus, the apparent slow rate of H-atom transfer is not surprising. Using our recent report that the cross relation (eq 1) can apply to hydrogen-atom transfer reactions,[8] we used three different reactions to estimate $k_{Co,H\bullet}$ (Table 5). The agreement among these three is poor, with values ranging from 10^{-3} to 10^{-9} M^{-1} s^{-1}. Perhaps one or more of these reactions occurs by an inner-sphere mechanism or there is some other breakdown of the cross relation.[8] It should be noted, however, that a value of 10^{-6} M^{-1} s^{-1} for $k_{Co,H\bullet}$ would give only 30-fold deviations in calculated cross rates. Despite this uncertainty, it is clear that hydrogen-atom self-exchange is at least 10^6 times slower for the cobalt biimidazoline complexes than for the Fe−H$_2$bim and Fe−H$_2$bip systems. The spin state change and large reorganization energy of the Co^{II}/Co^{III} couple inhibit the H-atom self-exchange as well as electron self-exchange.

(38) See the following and references therein: (a) Kohen, A.; Klinman, J. P. *Acc. Chem. Res.* **1998**, *31*, 397−404. (b) Huynh, M. H. V.; Meyer, T. J. *Angew. Chem., Int. Ed.* **2002**, *41*, 1395−8. (c) Mahapatra, S.; Halfen, J. A.; Tolman, W. B. *J. Am. Chem. Soc.* **1996**, *118*, 11575−11586. (d) Reinaud, O. M.; Theopold, K. H. *J. Am. Chem. Soc.* **1994**, *116*, 6979−6980. (e) Farrer, B. T.; Thorp, H. H. *Inorg. Chem.* **1999**, *38*, 2497. (f) Lewis, E. R.; Johansen, E.; Holman, T. R. *J. Am. Chem. Soc.* **1999**, *121*, 1395−6.

(39) See, for instance: (a) Peters, K. S.; Cashin, A.; Timbers, P. *J. Am. Chem. Soc.* **2000**, *122*, 107−113. (b) Kiefer, P. M.; Hynes, J. T. *J. Phys. Chem. A* **2002**, *106*, 1850−1861 and references therein. (c) Villa, J.; Corchado, J. C.; Gonzalez-Lafont, A.; Lluch, J. M.; Truhlar, D. G. *J. Phys. Chem. A* **1999**, *103*, 5061−5074 and references therein. (d) Krishtalik, L. I. *Biochim. Biophys. Acta* **2000**, *1458*, 6.

(40) (a) Bell, R. P. *The Tunnel Effect in Chemistry*; Chapman and Hall: New York, 1980; Chapter 4. (b) Kwart, H. *Acc. Chem. Res.* **1982**, *15*, 401−8.

(41) Jonsson, T.; Glickman, M. H.; Sun, S.; Klinman, J. P. *J. Am. Chem. Soc.* **1996**, *118*, 10319−10320.

(42) The ΔE_a is unlikely to result from differences in the spin-equilibria where deuteration should have little effect. Magnetic properties of **Fe^{II}(H$_2$bip)** and **Fe^{II}(D$_2$bip)-d_6** are the same within experimental error.

(43) Potentials vs Cp$_2$Fe$^{+/o}$ in MeCN: $E^{\circ\prime} = -0.55$ V for [Fe(H$_2$bip)]$_3{}^{2+/3+}$,[8,29] $E_{p,c} = -0.69$ V for irreversible reduction of **[Fe^{III}(Hbip)]**.

(44) For instance, electron self-exchange for [Co(sepulchrate)$_3$]$^{2+/3+}$ (5.1 $\pm$ 0.3 M^{-1} s^{-1} at 298 K) is faster than the typical Co^{II}/Co^{III} range apparently because the change in Co−N bond lengths is minimized: Creaser, I. I.; Harrowfield, J. M.; Herlt, A. J.; Sargeson, A. M.; Springborg, J.; Geue, R. J.; Snow, M. R. *J. Am. Chem. Soc.* **1977**, *99*, 3181.

(45) Endicott, J. F.; Ramasami, T. *J. Phys. Chem.* **1986**, *90*, 3740−3747.

Table 5. Estimates of the Hydrogen-Atom Self-Exchange Rate Constant for **Co^{II}(H$_2$bim)** + **Co^{III}(H$_2$bim)**, $k_{Co,H•}$, Calculated Using the Cross Relation (Eq 1)[a]

reaction	k[b]	K_{eq}	$k_{RO•+ROH}$	$k_{Co,H•}$(calcd)
Co^{II}(H$_2$bim) + ^{t}Bu$_3$C$_6$H$_2$O•	38 ± 5	6×10^6	$2.2 \times 10^{2\,c}$	10^{-6}
Co^{II}(H$_2$bim) + TEMPO•	$(2.8 \pm 0.6) \times 10^{-5}$	1×10^{-2}	$7 \times 10^{1\,d}$	10^{-9}
Co^{III}(Hbim) + HOC$_6$H$_4$OH	$(1.5 \pm 0.5) \times 10^{-3}$	1×10^{-7}	$3 \times 10^{4\,e}$	10^{-3}

[a] Rate constants (M^{-1} s^{-1}) and equilibrium constants in MeCN solvent, 298 K, ionic strength 0.05–0.1 M unless otherwise noted. Data from refs 8 and 29. [b] Rate constant per hydrogen. [c] CCl$_4$ solvent; ref 46. [d] Reference 29. [e] k_{SE}(3,6-^{t}Bu$_2$catechol/3,6-^{t}Bu$_2$orthosemiquinone radical) in CCl$_4$ solvent, ref 47.

The cobalt reactions are slow enough that the reactions of **Co^{II}(H$_2$bim)-d_{24}** with either **Co^{III}(H$_2$bim)** or **Co^{III}(Hbim)** occur by an alternative pathway involving a bridging biimidazoline ligand. Mass spectral results show incorporation of H$_2$bim-d_{24} into the Co^{III} derivatives despite their inertness toward substitution. Presumably a Hbim or H$_2$bim ligand on Co(III) acts as a ligand to labile **Co^{II}(H$_2$bim)**. This is quite reasonable for **Co^{III}-(Hbim)**, which has a deprotonated nitrogen on the outside of the ligand, but more difficult to picture for **Co^{III}(H$_2$bim)**.

Conclusions and Comments

Rate constants for degenerate hydrogen-atom exchange between [Fe^{II}(H$_2$bip)$_3$]$^{2+}$ and [Fe^{III}(Hbip)(H$_2$bip)$_2$]$^{2+}$ and degenerate electron exchange between [Fe^{II}(H$_2$bip)$_3$]$^{2+}$ and [Fe^{III}(H$_2$bip)$_3$]$^{3+}$ show quite unusual negative enthalpies of activation at temperatures near ambient (Table 4). From 240–288 K, electron self-exchange shows a more normal positive $\Delta H^{\ddagger}$. The negative $\Delta H^{\ddagger}$ appears to be due to the reactions occurring preferentially via the low-spin forms of the Fe(II) and Fe(III) derivatives, which are present in lower concentrations at higher temperatures. The deuterium atom is transferred more slowly than hydrogen ($k_H/k_D = 1.6 \pm 0.5$ at 298 K), with a similar or even more negative $\Delta H^{\ddagger}$. Although the error bars are large, the data appear inconsistent with a normal semiclassical origin for the isotope effect and suggest that both H and D transfers occur by tunneling mechanisms.[16,38–40]

In the Fe/H$_2$bip system, hydrogen-atom transfer is 10 times slower than electron exchange at 298 K (Table 4). The related Fe/H$_2$bim system has similar rate constants, with H-atom and electron self-exchange differing by a factor of 3. Self-exchange reactions of analogous cobalt-H$_2$bim complexes are dramatically slower. Direct measurements are not possible because inner-sphere pathways are preferred for both H• and e$^-$ self-exchange, but estimates have been obtained using the cross relation (eq 1): $10^{-9} \lesssim k_{Co,H•} \lesssim 10^{-3}$ M^{-1} s^{-1}, $k_{Co,e-} \cong 10^{-6}$ M^{-1} s^{-1}. Thus, in all three systems, there is a strong similarity between the electron and hydrogen-atom self-exchange reactions.

We suggest that, in general, factors that influence electron transfer will also affect hydrogen-atom transfer/proton-coupled electron transfer. The features that make Co^{II}/Co^{III} electron transfer very slow – the high-spin/low-spin interconversion and the large change in Co–N bond lengths – also slow hydrogen-atom transfer reactions involving the Co^{II}/Co^{III} redox couple. The preference for reaction of the low-spin iron complexes leads to unusual temperature dependencies for both electron and H-atom self-exchange.

However, the correspondence between electron and H-atom self-exchange observed here should not be considered a general rule. For example, Protasiewicz and Theopold showed that electron transfer between ^{n}Bu$_4$N[Tp^{Me2}Mo(CO)$_3$] and Tp^{Me2}-Mo(CO)$_3$ occurs rapidly ($k_{e-} = 8.6 \times 10^6$ M^{-1} s^{-1} at 303 K), while H-atom transfer between Tp^{Me2}Mo(CO)$_3$H and Tp^{Me2}Mo-(CO)$_3$ is very slow ($k_{H•} < 9.0 \times 10^{-3}$ M^{-1} s^{-1} at 239 K).[48] The slow H-atom transfer is likely a result of the significant intrinsic barrier for proton self-exchange in this system, as indicated by the slow rate constant $k_{H+} = 3.5$ M^{-1} s^{-1} at 303 K. In general, H-atom transfer involves moving both an electron and a proton, so it will be influenced by factors that affect either the electron or the proton transfer.

Experimental Section

All manipulations were performed using standard high-vacuum line, Schlenk, or cannula techniques, or in a glovebox under a nitrogen atmosphere.[49] Solvents were stored under vacuum over CaH$_2$ or Na/Ph$_2$CO. NMR spectra were obtained in CD$_3$CN at 298 K using a Brüker WM-500 spectrometer unless otherwise noted (DRX-499, AF-300, and AC-200 machines were also used). Chemical shifts are reported relative to residual solvent protons at 298 K unless noted otherwise. Line widths were determined from Lorentzian functions using the NMR utilities software NUTS (Acorn software) and are reported in Hertz (estimated errors, ±10 Hz). Simulations of NMR experiments were performed using the commercially available software gNMR version 4.1. Temperature calibration of NMR probes was accomplished by Van Geet's method.[50] UV–vis spectra were obtained using Hewlett-Packard 5482A or 5483 spectrophotometers and are reported as λ_{max} in nm (ϵ, M^{-1} cm^{-1}). Rapid kinetic measurements were made using an OLIS USA stopped flow instrument equipped with the OLIS rapid scanning monochromator and UV–vis detector. Elemental analyses were performed by Atlantic Microlabs (Norcross, GA). Electrospray mass spectrometry was performed on an Esquire-LC electrospray ion trap mass spectrometer (Bruker/Hewlett-Packard). CV data were collected on a BAS CV-27 in MeCN/^{n}Bu$_4$PF$_6$ with a platinum working electrode (Pt auxiliary, Ag/AgNO$_3$ reference).

Magnetic susceptibilities were determined in CD$_3$CN solvent containing (Me$_3$Si)$_2$O as a standard (200:1) using the Evans ^{1}H NMR method at 499 MHz (Brüker DRX-499).[20] Solutions contained **Fe^{II}-(H$_2$bip)** (22 mM), **Fe^{III}(H$_2$bip)** (18 mM), or **Fe^{III}(Hbip)** (22 mM). An aliquot of the CD$_3$CN/(Me$_3$Si)$_2$O solution (50 mL) was placed in a sealed capillary within each J. Young NMR sample tube. Reported values include corrections for the diamagnetic susceptibilities of complexes[51] but not the solvent.[52] Data were collected every 10 K from 240 to 320 K (except for **Fe^{III}(Hbip)**, the lowest temperature was 250 K). Fitting the data, following ref 23, required limiting values for the high-spin and low-spin moments. These were taken as 5.2 and 0 μ_B for Fe^{II}, and 5.9 and 2.0 μ_B for Fe^{III}, based on literature precedents[22–24] and on optimizing the linearity of the van't Hoff plots.

Reagents were purchased from Aldrich and purified by standard procedures[53] unless otherwise noted. Acetonitrile (Burdick and Jackson, Low-water brand) was stored in an argon-pressurized stainless steel drum and plumbed into the glovebox, via stainless steel tubing. Dimethyl sulfoxide (DMSO, Burdick and Jackson Biosyn brand) was

(46) Arick, M. R.; Weissman, S. I. *J. Am. Chem. Soc.* **1968**, *90*, 1654.
(47) Zavelovich, E. B.; Prokof'ev, A. I. *Chem. Phys. Lett.* **1974**, *29*, 212.
(48) Protasiewicz, J. D.; Theopold, K. H. *J. Am. Chem. Soc.* **1993**, *115*, 5, 5559–5569.
(49) Burger, B. J.; Bercaw, J. E. In *New Developments in the Synthesis, Manipulation, and Characterization of Organometallic Compounds*; Wayda, A.; Darensbourg, M. Y., Eds.; American Chemical Society: Washington, DC, 1987; Vol. 357.
(50) Van Geet, A. L. *Anal. Chem.* **1968**, *40*, 2227–2229.
(51) O'Connor, C. J. *Prog. Inorg. Chem.* **1982**, *29*, 203–283.
(52) Grant, D. H. *J. Chem. Educ.* **1995**, *72*, 39–40.
(53) Perrin, D. D.; Armarego, W. L. F. *Purification of Laboratory Chemicals*, 3rd ed.; Pergamon: New York, 1988.

stored under N_2 and used without further purification. Perchlorate salts were obtained as hydrates (Aldrich) and stored over $CaCl_2$. Deuterium enriched reagents were purchased from Cambridge Isotope Laboratories and were used as received, except for $(CD_3)_2SO$ which was dried by distillation from CaH_2 and stored over 4 Å molecular sieves, and CD_3-CN which was dried over P_2O_5 and CaH_2. 2,2′-Bitetrahydropyrimidine (H_2bip)[19] and 2,2′-biimidazoline (H_2bim)[25] were prepared according to the literature procedures (H_2bim-d_8 from $H_2NCD_2CD_2NH_2$).

Caution: The perchlorate salts described below are explosive and should be handled with care and in small quantities. They should not be heated when dry or subjected to friction or shock, such as scratching with a non-Teflon-coated spatula.

[Fe^{II}(H$_2$bip)$_3$](ClO$_4$)$_2$ [Fe^{II}(H$_2$bip)].[19] A 100 mL round-bottom flask was charged with H_2bip (971 mg, 6.0 mmol) and EtOH (80 mL). [Fe-$(H_2O)_6$](ClO$_4$)$_2$ (700 mg, 2.7 mmol) was added to a second flask. The use of excess iron is a modification of the literature procedure[19] and was necessary in our hands to avoid deprotonation of **Fe^{II}(H$_2$bip)** by H_2bip, which reduces the purity of the product. The two flasks were attached to opposite ends of a swivel frit apparatus and degassed. Heating the ligand solution to ∼50 °C caused ∼10 mL of EtOH to reflux into the flask containing the iron salt. The resulting iron solution was filtered into the ligand solution, resulting in an immediate color change to dark purple. The solution was allowed to cool to room temperature, and, over the course of 2 h, a purple solid deposited which was isolated by filtration and washed with EtOH. For safety reasons, the solids were separated into portions and dried, yielding 1.1 g (1.5 mmol, 75% based on ligand) of material. Repeated recrystallizations at −30 °C (MeCN layered with Et$_2$O) yielded 50% of pure microcrystalline material. ^{1}H NMR: δ −1.5 (6 C*H* [330]), 11.1 (6 C*H* [200]), 15.8 (6 C*H* [210]), 16.2 (6 C*H* [210]), 20.0 (6 C*H* [180]), 22.5 (6 C*H* [360]), 75.1 (6 N*H* [140]). ^{13}C NMR (125.8 MHz): δ −38.9 (s, *C*=N [120]), 89.8 (t, *C*H$_2$, $^1J_{CH}$ = 140 Hz), 92.6 (s, *C*H$_2$ [300]), 223.3 (s, *C*H$_2$ [315]). UV−vis (MeCN): 510 (2500), 580 (2300); Beer's law is followed between 0.28 and 0.07 mM. Anal. Calcd for C$_{24}$H$_{42}$Cl$_2$FeO$_8$N$_{12}$: C, 38.26; H, 5.61; N, 22.31. Found: C, 37.65; H, 5.47; N, 21.75.

[Fe^{III}(H$_2$bip)$_3$](ClO$_4$)$_3$ [Fe^{III}(H$_2$bip)].[19] In a modification of the literature procedure,[19] **Fe^{III}(H$_2$bip)** was prepared following the procedure for **Fe^{II}(H$_2$bip)** utilizing Fe^{III}(ClO$_4$)$_3$·xH$_2$O (365 mg, 1.0 mmol) and H_2bip (400 mg, 2.4 mmol) in EtOH (80 mL). Exclusion of air is not necessary for this preparation; excess iron reagent is used to prevent formation of **Fe^{III}(Hbip)**. After filtration, the orange to brown crude product was dried in vacuo and recrystallized twice from MeCN/Et$_2$O at −30 °C giving orange microcrystals in 30% yield. ^{1}H NMR: δ 3.1 (N*H* [130]), 9.8 (C*H* [280]), 12.3 (C*H* [270]), 20.8 (C*H* [∼2000]), 27.3 (C*H* [180]), 32.1 (C*H* [230]), 35.2 (C*H* [ca. 1000]); all signals have equal integration. UV−vis (MeCN): 476 (1900), 504 (2000). Anal. Calcd for C$_{24}$H$_{42}$Cl$_3$FeO$_{12}$N$_{12}$: C, 33.77; H, 4.97; N, 19.70. Found: C, 33.90; H, 5.04; N, 19.71.

[Fe^{III}(Hbip)(H$_2$bip)$_2$](ClO$_4$)$_2$ [Fe^{III}(Hbip)]. In a modification of the literature procedure,[19] a solution of **Fe^{II}(H$_2$bip)** (100 mg, 0.13 mmol) in MeCN (150 mL) was exposed to O$_2$ at 25 °C, resulting in a color change from purple to blue/green. After 1 h, the solvent was evaporated, and the resulting solid was recrystallized from MeCN/Et$_2$O; yield ∼75%. Product purity was checked by protonation with dilute solutions of HClO$_4$ in MeCN, with UV−vis spectroscopy confirming quantitative conversion to **Fe^{III}(H$_2$bip)**. UV−vis (MeCN): 390 (4700), 636 (3000). Anal. Calcd for C$_{24}$H$_{41}$Cl$_2$FeO$_8$N$_{12}$: C, 38.29; H, 5.51; N, 22.33. Found: C, 38.08; H, 5.42; N, 22.08.

[Co^{II}(H$_2$bim)$_3$](ClO$_4$)$_2$ [Co^{II}(H$_2$bim)]. In a modification of the literature procedure[25] for [Co^{II}(H$_2$bim)$_3$](NO$_3$)$_2$, a swivel frit apparatus was charged with H_2bim (365 mg, 2.64 mmol) and EtOH (65 mL) on one side and [Co(H$_2$O)$_6$](ClO$_4$)$_2$ (320 mg, 0.87 mmol) on the other. The ligand solution was heated to ∼50 °C with stirring, and EtOH (∼10 mL) was allowed to reflux into the flask containing the cobalt salt. The resulting solution of Co(ClO$_4$)$_2$ was then filtered into the ligand

solution, resulting in an immediate color change to light orange. The solution was allowed to cool to room temperature, and after 2 h it was reduced to dryness. MeCN (∼10 mL) was added by vacuum transfer, the dark orange mixture was filtered, and the solution was layered with Et$_2$O (∼30 mL) at −35 °C and allowed to come slowly to room temperature over a period of 9 h, yielding orange prisms (405 mg, 0.60 mmol, 70%). Crystals used for X-ray diffraction studies were grown at −30 °C using the slow diffusion technique described above. **Co^{II}(H$_2$bim)-d_{24}** was prepared in a similar manner from H_2bim-d_8. [Co^{II}(H$_2$bim)$_3$]Cl$_2$ can be prepared in an analogous manner using dry CoCl$_2$. ^{1}H NMR: δ 21.2 (C*H*, 12 H [40]), 35.3 (N*H*, 6 H [110]), 52.0 (C*H*, 12 H [150]). Magnetic susceptibility: 4.5 μ_B. UV−vis (MeCN): 485 (46). Anal. Calcd for C$_{18}$H$_{30}$Cl$_2$CoO$_8$N$_{12}$: C, 32.13; H, 4.51; N, 24.99. Found: C, 32.37; H, 4.56; N, 24.97. The dichloride salt [Co^{II}(H$_2$-bim)$_3$](Cl)$_2$ was prepared from CoCl$_2$ according to the procedure for the nitrate salt.[25]

[Co^{III}(H$_2$bim)$_3$](ClO$_4$)$_3$ [Co^{III}(H$_2$bim)]. MeCN (180 mL) was added to a flask wrapped with Al foil containing AgClO$_4$ (820 mg, 3.67 mmol) and [Co^{II}(H$_2$bim)$_3$]Cl$_2$ (670 mg, 1.23 mmol) {[Co^{II}(H$_2$bim)$_3$](ClO$_4$)$_2$ can also be used}. After the mixture was stirred for 12 h, the solvent was evaporated. MeCN (∼60 mL) was added, and the solution was allowed to stand for 2 days exposed to light. Filtration to remove AgCl and Ag° afforded a red/pink solution which was reduced to ∼15 mL and layered with Et$_2$O (∼35 mL) at −35 °C. After being warmed to room temperature over a period of 9 h, red/pink plates were isolated by filtration and dried in vacuo (850 mg, 1.10 mmol, 90%). Elemental analysis and X-ray diffraction both indicate one acetonitrile molecule for every three cobalt(III) ions. When less than 3 equiv of AgClO$_4$ was reacted with the dichloride salt, the yield was reduced, but fewer recrystallizations were required for purification. ^{1}H NMR: δ 3.6 (m, C*H*, 12 H), 4.0 (m, C*H*, 12 H), 7.3 (s, N*H*, 6 H). ^{13}C{^{1}H} NMR (75.5 MHz): δ 47.5 (*C*H$_2$), 49.6 (*C*H$_2$), 160.6 (*C*=N). UV−vis (MeCN): 510 (310). Anal. Calcd for C$_{18.7}$H$_{31}$Cl$_3$CoO$_{12}$N$_{12.3}$: C, 28.58; H, 3.99; N, 21.93. Found: C, 28.85; H, 4.08; N, 22.01.

[Co^{III}(Hbim)(H$_2$bim)$_2$](ClO$_4$)$_2$ [Co^{III}(Hbim)]. MeCN (10 mL) was vacuum transferred into a flask containing **Co^{III}(H$_2$bim)** (97 mg, 0.13 mmol) and LiN^{i}Pr$_2$ (15 mg, 0.14 mmol). The reaction was stirred for 10 min at room temperature. The solvent was then evaporated giving a dark red, oily solid. A 1:1 mixture of MeCN:Et$_2$O was then added, and the resulting green/brown solid was isolated by filtration from the red solution. The solid was washed with Et$_2$O and dried in vacuo affording **Co^{III}(Hbim)** (40 mg, 47%). ^{1}H NMR: δ 3.3 (m, C*H*, 6 H), 3.6 (m, C*H*, 6 H), 4.0 (m, C*H*, 12 H), 5.4 (s, N*H*, 5 H). UV−vis (MeCN): 450 (1000), 586 (600).

^{1}H NMR Measurement of Self-Exchange Rate Constants. Method 1: A stock solution of **Fe^{II}(H$_2$bip)** in CD$_3$CN was apportioned equally between two J. Young NMR tubes. ^{1}H NMR spectra were acquired to establish reagent and solution purity. In a glovebox, both tubes were opened, and a stock solution of either **Fe^{III}(Hbip)** or **Fe^{III}(H$_2$bip)** in CD$_3$CN was added to only one tube. ^{1}H NMR spectra were then acquired for both. This procedure minimizes errors (spurious broadening) resulting from aerobic conversion of **Fe^{II}(H$_2$bip)** to **Fe^{III}(Hbip)**. The line widths for resonances were measured using fits to a Lorentzian line shape with NUTS; ΔW for eq 6 is the difference in line width between the two tubes.

Method 2: A stock solution of **Fe^{II}(H$_2$bip)** in CD$_3$CN was apportioned equally between five J. Young NMR tubes. Stock solutions of **Fe^{III}(Hbim)** or **Fe^{III}(H$_2$bim)** in CD$_3$CN were then added to four of the tubes in varying amounts. ^{1}H NMR spectra were acquired, and the line widths were fit as above. Rate constants measured using these two methods were the same within experimental error. In some experiments, the ionic strengths were kept constant (83 mM for electron transfer and 74 mM for H-atom), while in others they varied from one tube to another (74−100 mM for electron, 104−125 mM for H-atom, and 60−80 mM for D-atom exchange).

Deuterium self-exchange rates were measured by method 2 and are corrected for the 94% D, 6% H composition of the materials. **Fe^{II}-(D$_2$bip)-d_6** was prepared by triple exchange of **Fe^{II}(H$_2$bip)** with CH$_3$-OD and was oxidized with O$_2$ to give **Fe^{II}(Hbip)-d_5**.

In the reaction of **Co^{II}(H$_2$bim)-d_{24} + Co^{III}(Hbim)**, mass clusters were observed for Co(II) derivatives centered at 434 ([Co(H$_2$bim)$_2$-(ClO$_4$)]$^+$), 442 ([Co(H$_2$bim)(H$_2$bim-d_8)ClO$_4$]$^+$), and 450 ([Co(H$_2$bim-d_8)$_2$(ClO$_4$)]$^+$), and for Co(III) at 471 ([Co(Hbim)$_2$(H$_2$bim)]$^+$), 479 ([Co(Hbim)$_2$(H$_2$bim-d_8)]$^+$), 487 ([Co(Hbim)(Hbim-d_8)(H$_2$bim-d_8)]$^+$), and 495 ([Co(Hbim-d_8)$_2$(H$_2$bim-d_8)]$^+$). In the reaction of **Co^{II}(H$_2$bim)-d_{24} + Co^{III}(H$_2$bim)**, four mass clusters were observed for Co(III) at 671 ([Co(H$_2$bim)$_3$(ClO$_4$)$_2$]$^+$), 679 ([Co(H$_2$bim)$_2$(H$_2$bim-d_8)(ClO$_4$)$_2$]$^+$), 687 ([Co(H$_2$bim)(H$_2$bim-d_8)$_2$-(ClO$_4$)$_2$]$^+$), and 695 ([Co(H$_2$bim-d_8)$_3$-(ClO$_4$)$_2$]$^+$), in addition to those for the Co(II) compounds.

Errors limits in rate constants and activation parameter are reported as ±2 s. The largest source of error associated with the ^{1}H NMR lifetime measurements derives from changes in Lorentzian line shape. Spurious broadening of the **Fe^{II}(H$_2$bip)** signals may result from magnetic field inhomogeneity, differences in probe temperature, and the presence of trace impurities. Comparison of **Fe^{II}(H$_2$bip)** samples, prepared on different days in different tubes using different source materials, indicates ±8% variation in the natural line widths at δ 11.1 and −1.5. Errors in solution concentrations were estimated to be ±2%. The error in k (defined by eq 6) was propagated with respect to changes in line-broadening ($\Delta\Delta$fwhm) and Fe^{III} concentration (Δ[Fe^{III}]) using eq 12.[54] Error-weighted rate constants were used in the fitting of the data to the Arrhenius expression, and eqs 13 and 14[54] were used to assess the root-mean-square error $\Delta(E_a^H) - E_a^D$ and the propagated error Δ-(A^H/A^D).

$$(\Delta k) = \sqrt{(\partial k/\partial\Delta\text{fwhm})^2(\Delta\Delta\text{fwhm})^2 + (\partial k/\partial[\text{Fe}^{III}])^2(\Delta[\text{Fe}^{III}])^2} \tag{12}$$

$$\Delta(E_a^H - E_a^D) = \sqrt{(\Delta E_a^H)^2 + (\Delta E_a^D)^2} \tag{13}$$

$$\Delta(A^H - A^D) = \sqrt{(1/A^D)^2(\Delta A^H)^2 + [-A^H/(A^D)^2](\Delta A^D)^2} \tag{14}$$

Stopped Flow Kinetics. MeCN solutions of reagents **Co^{III}(H$_2$bim)**, ~2 mM, and **Fe^{II}(H$_2$bim)**, ~0.1 mM, were loaded into syringes in the glovebox. The OLIS stopped flow apparatus was flushed with 15−20 mL of MeCN, and a background spectrum was acquired. The syringes containing the reagents were then attached, and the apparatus was flushed with approximately 5−7 mL of reagent solutions. Slight exposure to air was unavoidable but in most cases did not adversely affect the reactions. A kinetic trace was then acquired, and the reaction was repeated two or three times. Reactions were typically run under pseudo-first-order conditions, and observed rate constants were extracted either using single wavelength fits to an exponential function or using the OLIS global fitting program.

X-ray Crystal Structures of Co^{II}(H$_2$bim) and Co^{III}(H$_2$bim). Crystals were grown at −30 °C in MeCN in a glove box. Data were collected using a Nonius Kappa CCD with Mo Kα radiation. Crystals were mounted in glass capillary tubes in epoxy or oil. Crystal to detector distances were 27 mm, and exposure times were 20 s for **Co^{II}(H$_2$bim)** (three exposures) and 315 s for **Co^{III}(H$_2$bim)** (six exposures). Data reduction and cell refinement were done with Denzo-SMN and HKL SCALEPACK,[55] and absorption corrections were introduced with SORTAV.[56] Direct methods were employed using SIR92 and SHELXL-97.[57] Non-hydrogen atoms were refined anisotropically by a full-matrix least-squares method. Hydrogen atoms were located from difference maps and refined with a riding model, except as noted. For **Co^{III}-(H$_2$bim)**, racemic twinning (50/50) was discovered and introduced.

Supporting Information Available: Crystallographic data (CIF format) for **[Co^{II}(H$_2$bim)]** and **[Co^{III}(H$_2$bim)]**. This material is available free of charge via the Internet at http://pubs.acs.org.

(54) Steinfeld, J. I.; Francisco, J. S.; Hase, W. L. *Chemical Kinetcis and Dynamics*; Prentice Hall: New Jersey, 1989; pp 136−142

(55) Otinowski, Z.; Minor, W. *Methods Enzymol.* **1996**, *276*, 307−326.
(56) Blessing, R. H. *Acta Crystallogr.* **1995**, *A51*, 33.
(57) Altomare, A.; Cascarano, G.; Giacovazzo, C.; Burla, M. C.; Polidori, G.; Camalli, M. *J. Appl. Crystallogr.* **1994**, *27*, 435−442. Sheldrick, G. M. *SHELXL-97*; University of Gottingen, Germany, 1997.